The Plant Cell, Vol. 28: 2291–2311, September 2016, www.plantcell.org

FYVE1/FREE1 Interacts with the PYL4 ABA Receptor and Mediates Its Delivery to the Vacuolar Degradation Pathway

Borja Belda-Palazon,[a,1] Lesia Rodriguez,[a,1] Maria A. Fernandez,[a] Mari-Cruz Castillo,[a] Erin M. Anderson,[b] Caiji Gao,[c] Miguel Gonzalez-Guzman,[a] Marta Peirats-Llobet,[a] Qiong Zhao,[c] Nancy De Winne,[d] Kris Gevaert,[e] Geert De Jaeger,[d] Liwen Jiang,[c] José León,[a] Robert T. Mullen,[b] and Pedro L. Rodriguez[a,2]

[a] Instituto de Biología Molecular y Celular de Plantas, Consejo Superior de Investigaciones Científicas-Universidad Politécnica de Valencia, 46022 Valencia, Spain

[b] Department of Molecular and Cellular Biology, University of Guelph, Guelph, Ontario N1G 2W1, Canada

[c] Centre for Cell and Developmental Biology and State Key Laboratory of Agrobiotechnology, School of Life Sciences, The Chinese University of Hong Kong, Hong Kong, China

[d] Department of Plant Systems Biology and Department of Plant Biotechnology and Bioinformatics, Vlaams Instituut voor Biotechnologie, Ghent University, B-9052 Ghent, Belgium

[e] Department of Medical Protein Research and Department of Biochemistry, Vlaams Instituut voor Biotechnologie, Ghent University, B-9000 Ghent, Belgium

ORCID IDs: 0000-0003-0601-6735 (L.R.); 0000-0002-9647-0896 (M.-C.C.); 0000-0003-1000-9255 (M.G.-G.); 0000-0003-4557-3139 (Q.Z.); 0000-0002-4237-0283 (K.G.); 0000-0001-6558-5669 (G.D.J.); 0000-0002-7332-1572 (J.L.); 0000-0002-6915-7407 (R.T.M.); 0000-0002-5886-9425 (P.L.R.)

Recently, we described the ubiquitylation of PYL4 and PYR1 by the RING E3 ubiquitin ligase RSL1 at the plasma membrane of *Arabidopsis thaliana*. This suggested that ubiquitylated abscisic acid (ABA) receptors might be targeted to the vacuolar degradation pathway because such ubiquitylation is usually an internalization signal for the endocytic route. Here, we show that FYVE1 (previously termed FREE1), a recently described component of the endosomal sorting complex required for transport (ESCRT) machinery, interacted with RSL1-receptor complexes and recruited PYL4 to endosomal compartments. Although the ESCRT pathway has been assumed to be reserved for integral membrane proteins, we show the involvement of this pathway in the degradation of ABA receptors, which can be associated with membranes but are not integral membrane proteins. Knockdown *fyve1* alleles are hypersensitive to ABA, illustrating the biological relevance of the ESCRT pathway for the modulation of ABA signaling. In addition, *fyve1* mutants are impaired in the targeting of ABA receptors for vacuolar degradation, leading to increased accumulation of PYL4 and an enhanced response to ABA. Pharmacological and genetic approaches revealed a dynamic turnover of ABA receptors from the plasma membrane to the endosomal/vacuolar degradation pathway, which was mediated by FYVE1 and was dependent on RSL1. This process involves clathrin-mediated endocytosis and trafficking of PYL4 through the ESCRT pathway, which helps to regulate the turnover of ABA receptors and attenuate ABA signaling.

INTRODUCTION

The phytohormone abscisic acid (ABA) plays fundamental roles in the regulation of plant growth and development, as well as in plant stress responses. ABA elicits plant responses through a complex signal transduction pathway that begins with ABA binding to soluble PYRABACTIN RESISTANCE1 (PYR1)/PYR1-LIKE (PYL)/REGULATORY COMPONENTS OF ABA RECEPTORS (RCAR) receptors, which constitute a multigene family. PYR/PYL/RCAR receptors perceive ABA either intracellularly or near the plasma membrane (Rodriguez et al., 2014; Diaz et al., 2016) and, as a result, form ternary complexes with clade A protein phosphatases type 2C (PP2Cs), thereby inactivating them (Park et al., 2009; Ma et al., 2009; Santiago et al., 2009). This prevents the PP2C-mediated dephosphorylation of ABA-activated sucrose nonfermenting 1-related protein kinases (SnRKs) subfamily 2 (SnRK2s) and results in the activation of a SnRK2-dependent phosphorylation cascade that affects a large number of targets in plant cells (Wang et al., 2013; Umezawa et al., 2013). Thus, ABA-activated SnRK2s regulate different cellular processes, including ion and water transport in plasma membrane and transcriptional response to ABA (Cutler et al., 2010; Finkelstein, 2013; Yoshida et al., 2015; Grondin et al., 2015; Peirats-Llobet et al., 2016).

Recent advances in the field of ABA signaling have shown that PYR/PYL ABA receptors are subjected to ubiquitylation, either in the nucleus by the CULLIN4-RING E3 ubiquitin ligase complex formed by COP10-DET1-DDB1 and the substrate adapter DDB1-ASSOCIATED1 (Irigoyen et al., 2014) or at the plasma membrane by the single subunit RING-type E3 ubiquitin ligase RSL1 (Bueso et al., 2014). In particular, RSL1 bears a C-terminal transmembrane domain that anchors the E3 ligase to the plasma membrane, where RSL1 interacts with PYL4 and PYR1 (Bueso et al., 2014). Ubiquitylation of plasma membrane proteins is usually an internalization signal for the endocytic route via the

[1] These authors contributed equally to this work.

[2] Address correspondence to prodriguez@ibmcp.upv.es.
The author responsible for distribution of materials integral to the findings presented in this article in accordance with the policy described in the Instructions for Authors (www.plantcell.org) is: Pedro L. Rodriguez (prodriguez@ibmcp.upv.es).

www.plantcell.org/cgi/doi/10.1105/tpc.16.00178

endosomal sorting complex required for transport (ESCRT) machinery, which mediates the delivery of proteins to the vacuolar degradation pathway (Murphy et al., 2005; Teis et al., 2009; Raiborg and Stenmark, 2009; Scheuring et al., 2012; MacGurn et al., 2012). Therefore, we suggested that ubiquitylation of ABA receptors at the plasma membrane by RSL1 might trigger endocytosis and ESCRT-mediated sorting for vacuolar degradation (Bueso et al., 2014).

During a combined tandem affinity purification (TAP)/mass spectrometry search for PYL4-interacting proteins, we identified a PYL4-interacting protein, At1g20110, which contains a FYVE domain. The FYVE domain is a phosphatidylinositol-3-phosphate (PI3P) binding motif named after four proteins that contain it: Fab1b, YOTB, Vac1p, and EEA1 (Gaullier et al., 1998; Lemmon, 2008). In mammalian and yeast cells, PI3P is found primarily in endosomes and phagosomes (Gaullier et al., 1998; Misra and Hurley, 1999; Lemmon, 2008), whereas in plant cells, PI3P is mainly enriched in prevacuolar compartment (PVC)/multivesicular bodies (MVBs) (Vermeer et al., 2006). FYVE domains are membrane-targeting regions highly specific for PI3P, and proteins containing the FYVE domain are primarily associated with functions related to endosomal trafficking and the ESCRT machinery (Stenmark et al., 2002).

At1g20110 was previously named FYVE1 and was identified as a factor involved in the recycling of IRON-REGULATED TRANSPORTER1 (IRT1) to the plasma membrane in *Arabidopsis thaliana* (Barberon et al., 2014). FYVE 1 was shown to bind PI3P and was partially localized to late endosomes (LEs) (Barberon et al., 2014). A survey of the Arabidopsis genome identified 15 FYVE domain-containing proteins, which were classified in five classes according to their domain architecture (Wywial and Singh, 2010). Interestingly, At1g20110/FYVE1 is the only member of class IV, and homozygous knockout *fyve1-1* seeds were unable to germinate and establish, suggesting that FYVE1 function is essential for viability (Barberon et al., 2014; Gao et al., 2014).

FYVE1 was also identified by Gao et al. (2014) in a search for plant FYVE domain-containing proteins that might perform an endosomal sorting-related function. Termed as FREE1 (FYVE-domain protein required for endosomal sorting 1) Gao et al. (2014) showed that FYVE1/FREE1 bound both ubiquitin and PI3P and that it interacted with Vps23A in order to be incorporated into the ESCRT-I complex. Because the name FYVE was published a few months before FREE, we will use FYVE in this article. Physiological characterization of FYVE1 has subsequently revealed a myriad of functions, including its roles in regulation of the formation of intraluminal vesicles (ILVs) in PVCs/MVBs, MVB-mediated sorting and degradation of ubiquitylated membrane proteins, vacuolar protein transport, autophagic degradation, and vacuole biogenesis (Gao et al., 2014, 2015; Kolb et al., 2015). Taken together, these processes reflect the key role of FYVE1 in endomembrane trafficking and, hence, in plant growth and development. In this work, we discovered an unexpected interaction of FYVE1 with PYR/PYL ABA receptors that delivers them as cargo to the ESCRT machinery. Because FYVE1 is a unique ESCRT component that binds ubiquitin and regulates vacuolar sorting of proteins, our results suggest that ubiquitylated ABA receptors are cargo for FYVE1 to mediate their delivery to the vacuolar degradation pathway.

RESULTS

FYVE1 Interacts with PYL4

In order to identify interacting partners of ABA receptors we used an in vivo biochemical/mass spectrometry approach using Arabidopsis suspension cells that stably express a protein G/streptavidin (GS)-tagged PYL4 as bait for TAP (Figure 1A). We performed TAP of protein complexes in GS-PYL4-expressing Arabidopsis cells that were mock or 50 μM ABA treated, and subsequent liquid chromatography-tandem mass spectrometry (LC-MS/MS) analysis on LTQ Orbitrap Velos of these complexes revealed a candidate PYL4-interacting protein, At1g20110/FYVE1/FREE1 (Figure 1A, Table 1; Supplemental Data Set 1). Alignment of At1g20110 and the FYVE domain of EEA1 revealed the three signature sequences that define the FYVE domain: a WxxD motif, a basic RRHHCR patch, and an RVC motif (Gaullier et al., 1998) (Supplemental Figure 1). In addition to FYVE1, four clade A PP2Cs (HAB1, ABI1, ABI2, and HAB2) were recovered as PYL4-interacting proteins when samples were supplemented with 50 μM ABA (Figure 1A, Table 1). The number of protein matches for FYVE1 was low (approximately 5% of total peptide matches) compared with clade A PP2Cs, probably because FYVE1 is mostly membrane associated (Gao et al., 2014)—the TAP approach was not optimized to this end—and clade A PP2Cs are the major interactors of ABA receptors (Antoni et al., 2013). Notably, in the absence of exogenous ABA supplementation, neither FYVE1 nor PP2Cs were recovered as PYL4-bound complexes (Supplemental Data Set 1).

FYVE1 encodes a protein of 601 amino acid residues and, according to PSIPRED and DISOPRED2 prediction servers (http://bioinf.cs.ucl.ac.uk/), the N-terminal portion of the protein contains an intrinsically disordered region (IDR) characterized by the presence of a Pro- and Gln-rich sequence that is ~200 amino acids long, whereas the FYVE domain is found in the C-terminal half of the protein (Figure 1B; Supplemental Figure 2). In order to identify the region of FYVE1 responsible of its interaction with PYR/PYLs, we generated N-terminal (amino acid residues 1 to 395, FYVE1^{N}) and C-terminal (residues 396 to 601, FYVE1^{C}) constructs in the GAD yeast two-hybrid vector and tested them for interaction with several PYL proteins. As shown in Figure 1B, neither GAD-FYVE1^{N} nor GAD-FYVE1^{C} led to autoactivation of the *HIS3* and *ADE2* reporter genes when cotransformed with GBD-empty vector (Figure 1B). However, GAD-FYVE1^{N} but not GAD-FYVE1^{C} interacted with all of the tested ABA receptors, both in the absence and presence of ABA. While we cannot exclude the possibility that the FYVE1^{C} construct might be targeted to membranes in yeast, precluding it from associating with PYR/PYLs in the yeast two-hybrid (Y2H) assay, the data obtained suggest that FYVE1^{N} interacts with ABA receptors in an ABA-independent manner.

FYVE1 is localized in endosomes and PVCs/MVBs in Arabidopsis protoplasts (Gao et al., 2014). Therefore, we performed bimolecular fluorescence complementation (BiFC) assays to determine the subcellular localization of the FYVE1-PYL4 interaction in tobacco leaf cells. Specifically, FYVE1 and PYL4 were translationally fused to either the N- or the C-terminal half of yellow fluorescent protein (YFP^{N} and YFP^{C}), and the corresponding

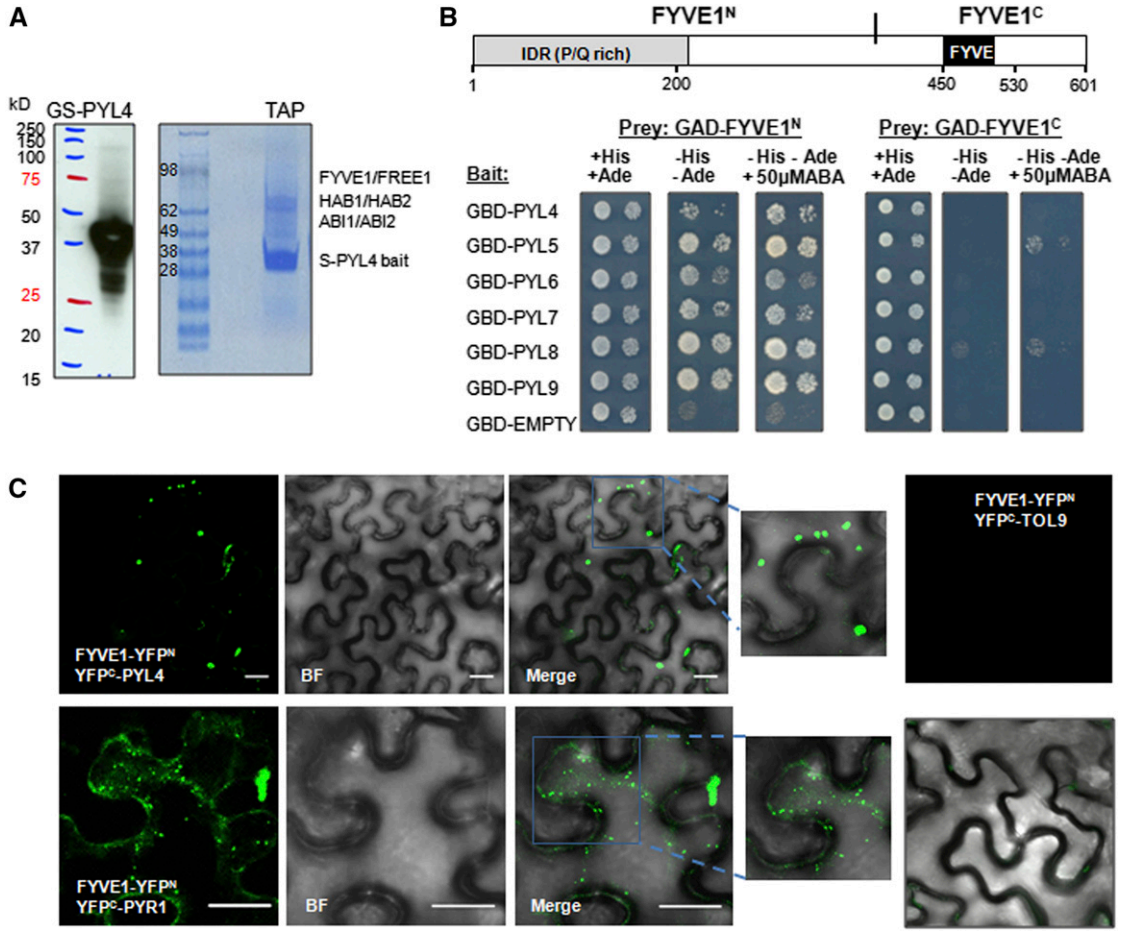

Figure 1. TAP/Mass Spectrometry and BiFC Analyses Reveal That PYL4 Interacts in Vivo with FYVE1.

(A) Expression of GS-PYL4 in Arabidopsis cell suspension cultures and recovery of PYL4-interacting proteins following TAP and mass spectrometry analysis. Immunoblot analysis using an anti-GS antibody detects the GS-PYL4 bait in Arabidopsis protein extracts prepared from transformed suspension cells (left panel). Coomassie blue staining reveals the presence of S-PYL4 eluted after the second purification step plus accompanying proteins (right panel). The different sizes of GS-PYL4 and S-PYL4 are due to TEV cleavage of the G domain after the first purification step.

(B) The structure of FYVE1 showing the N-terminal location of the IDR and the FYVE domain. Interaction of FYVE1 and PYL ABA receptors in Y2H assays was determined by growth assay on media lacking histidine and adenine. The presence of 50 μM ABA does not affect significantly the observed interaction.

(C) BiFC interaction of ABA receptors and FYVE1 decorates endosomes and MVB/PVC. Photographs show epifluorescence confocal images of transiently transformed tobacco epidermal cells coexpressing FYVE1-YFP^N and YFP^C-PYL4 or PYR1. The merging of the fluorescent (left panels) and bright-field (BF) images reveals the subcellular location of the interaction in endosomal compartments. FYVE1-YFP^N does not interact with YFP^C-TOL9 in a BiFC assay (far right panels). Bars = 20 μm.

fusion proteins were coexpressed in tobacco (*Nicotiana benthamiana*) cells via agroinfiltration. A confocal laser scanning microscopy (CLSM) 3D projection through a full *z*-series revealed that the FYVE1-PYL4 interaction occurred in small intracellular vesicles reminiscent of endosomes (Figure 1C). Because both PYL4 and PYR1 are ubiquitylated by RSL1 at the plasma membrane (Bueso et al., 2014), we also tested the interaction of PYR1 and FYVE1 by BiFC. We found that FYVE and PYR1 interact in tobacco cells, in regions reminiscent of endosomal and PVCs (Figure 1C). By contrast, FYVE-YFP^N coexpressed with YFP^C-TOL9 did not produce a BiFC signal (Figure 1C), whereas negative controls of YFP^C-PYR1/PYL4 have been published elsewhere (Santiago et al., 2009; Irigoyen et al., 2014; Rodriguez et al., 2014).

FYVE1 Connects the PYL4-RSL1 Complex with the ESCRT Machinery

The movement of membrane proteins to MVBs involves the binding of ubiquitylated cargos to the outer endosomal membrane and the recruitment of the ESCRT machinery (Winter and Hauser, 2006). The presence of GFP-RSL1 in endosomal compartments has been reported previously through colocalization with the VTI12/WAVE13 marker, which decorates TGN and early endosomes, and visualization of GFP-RSL1 in brefeldin A (BFA)-induced compartments (Bueso et al., 2014). Results shown in Figure 1C also suggest that ABA receptors follow endosomal trafficking. Given the reported role of the ESCRT component FYVE1 for the

Table 1. Proteins Identified by Mass Spectrometry after TAP of GS-PYL4

	Identified Proteins					
TAP	Locus	Name	Molecular Mass (D)	Protein Score	Protein Seq. Sig.	Sequence Coverage (%)
Mock	AT2G38310	PYL4	22,706	10,946	30	80
50 μM ABA	AT2G38310	PYL4	22,706	3,787	33	89
	AT1G72770	HAB1	56,393	1,092	24	31
	AT1G17550	HAB2	56,767	297	7	9
	AT4G26080	ABI1	47,989	592	14	19
	AT5G57050	ABI2	46,847	391	11	15
	AT1G20110	FYVE1	66,153	67	2	4

TAP was performed using protein extracts that were mock or 50 μM ABA treated according to the purification procedure described in Methods. LC-MS/MS analysis on LTQ Orbitrap Velos identified clade A PP2Cs and FYVE1 as interacting partners of PYL4.

formation of ILVs and the sorting of ubiquitylated membrane cargoes (Gao et al., 2015), we tested whether PYL4-RSL1 membrane complexes (Bueso et al., 2014) colocalized with FYVE1. Using BiFC assays, we visualized the interaction of SCYAN^N-RSL1 and SCYAN^C-PYL4 or PYR1 in plasma membrane and endosomal compartments of tobacco cells (Figure 2A). Coexpression of FYVE1-GFP with either the protein complex RSL1/PYL4 or RSL1/PYR1 (expressed as SCYAN^N-RSL1/SCYAN^C-PYL4 or PYR1) revealed colocalization of FYVE1-GFP with the SCYAN fluorescent signal (Figure 2A). To quantify colocalization results, the linear Pearson (Rp) and the nonlinear Spearman's (Rs) correlation coefficient were calculated using FIJI software (https://imagej.nih.gov) (French et al., 2008). The observed interaction of PYR/PYL ABA receptors and FYVE1 at endosomes and MVBs/PVCs suggests that FYVE1 might act to recruit PYR/PYL receptors for endosomal sorting once they are ubiquitylated by RSL1 at the plasma membrane.

In order to test whether the interaction of RSL1 and ABA receptors mediates their delivery to the vacuole of tobacco cells, we coexpressed RSL1/PYL4 or RSL1/PYR1 (as YFP^N-RSL1/YFP^C-PYL4 or PYR1) together with the vacuolar reporter RFP-TMD23-Ub and performed 3D projection through a full *z*-series of CLSM images (Scheuring et al., 2012). In addition to interaction at the plasma membrane and in endosomes/PVCs, a clear vacuolar fluorescent signal (reconstituted YFP) from the RSL1/PYL4 or RSL1/PYR1 complexes was seen, and this signal overlapped with the vacuolar pattern decorated by RFP-TMD23-Ub (Figure 2B).

These data suggest that the docking of ABA receptors to the plasma membrane by RSL1 targets them for vacuolar degradation and promotes the transport of the E3 ligase to the vacuole. Vacuolar delivery of GFP fusion proteins yields a characteristic vacuolar degradation product, termed GFP core (daSilva et al., 2005; Scheuring et al., 2012). We monitored vacuolar degradation of GFP-PYL4 by immunoblot analysis in Arabidopsis transgenic plants expressing GFP-PYL4 (Figure 2C). By comparing the production of the GFP core in mock versus E64 inhibitor of cysteine protease-treated seedlings, we found that E64, which stabilizes fluorescent proteins in the vacuolar compartment (Nodzynski et al., 2013), reduced the production of the GFP core and increased the GFP-PYL4 protein level (Figure 2C).

Transient interaction of ABA receptors with the plasma membrane is facilitated by their interaction with RSL1 as well as with C2-domain ABA-related (CAR) proteins (Rodriguez et al., 2014; Diaz et al., 2016). CAR proteins cluster on the membrane as peripheral proteins in a calcium-dependent manner through the C2 domain and polybasic lipid binding site, generating membrane curvature and providing a signaling platform involved in the docking of ABA receptors (Diaz et al., 2016). In order to investigate the possible relationship of CAR-Receptor complexes with FYVE1, we coexpressed CAR1, PYL4, or PYR1 and FYVE1 in tobacco cells (expressed as CAR1-YFP^N, YFP^C-Receptor, and RFP-FYVE1 fusion proteins). The interaction of PYL4 or PYR1 with CAR1 was visualized by BiFC as punctate/globular shaped structures in the plasma membrane that colocalize with a fraction of RFP-FYVE1 (Figure 2D; Supplemental Figure 3A). These results suggested that CAR1-PYR1 or PYL4 complexes in the plasma membrane might serve as a cargo for endosomal sorting mediated by FYVE1. However, CAR1-PYR1 or CAR1-PYL4 complexes were not found in the vacuole when coexpressed with RFP-TMD23-Ub under our experimental conditions (Supplemental Figure 3B).

FYVE1 Interacts in Planta with Vps23A ESCRT-I and Snf7A ESCRT-III Subunits

In Arabidopsis protoplasts, FYVE1 is incorporated into the ESCRT-I complex via direct interaction with Vps23A through PTAP-like motifs residing in the N-terminal Pro-rich region of FYVE1 (Gao et al., 2014). We confirmed this interaction in planta using BiFC assays in tobacco epidermal cells, which showed interaction of FYVE1 with Vps23A both in punctate and globular shaped structures (Supplemental Figure 4A). ESCRT comprises a set of proteins which are assembled at the endosomal membrane into several multiprotein subcomplexes, termed ESCRT-0, -I, -II, and -III (Paez Valencia et al., 2016). Trafficking of proteins ubiquitylated at the plasma membrane requires ESCRT to generate ILVs in MVBs, which ultimately will reach the vacuole for degradation. A key step in the formation of ILVs requires the ESCRT-III subunit Snf7A, which forms concentric filaments surrounding spherical membranes that are ultimately delivered into the endosomal lumen (Hanson and Cashikar, 2012; Cashikar et al., 2014). We performed BiFC assays of YFP^C-Snf7A and FYVE1-YFP^N proteins expressed in tobacco leaf cells by *Agrobacterium tumefaciens*-mediated transfection and observed interaction of FYVE1 and Snf7A in membrane compartments that are

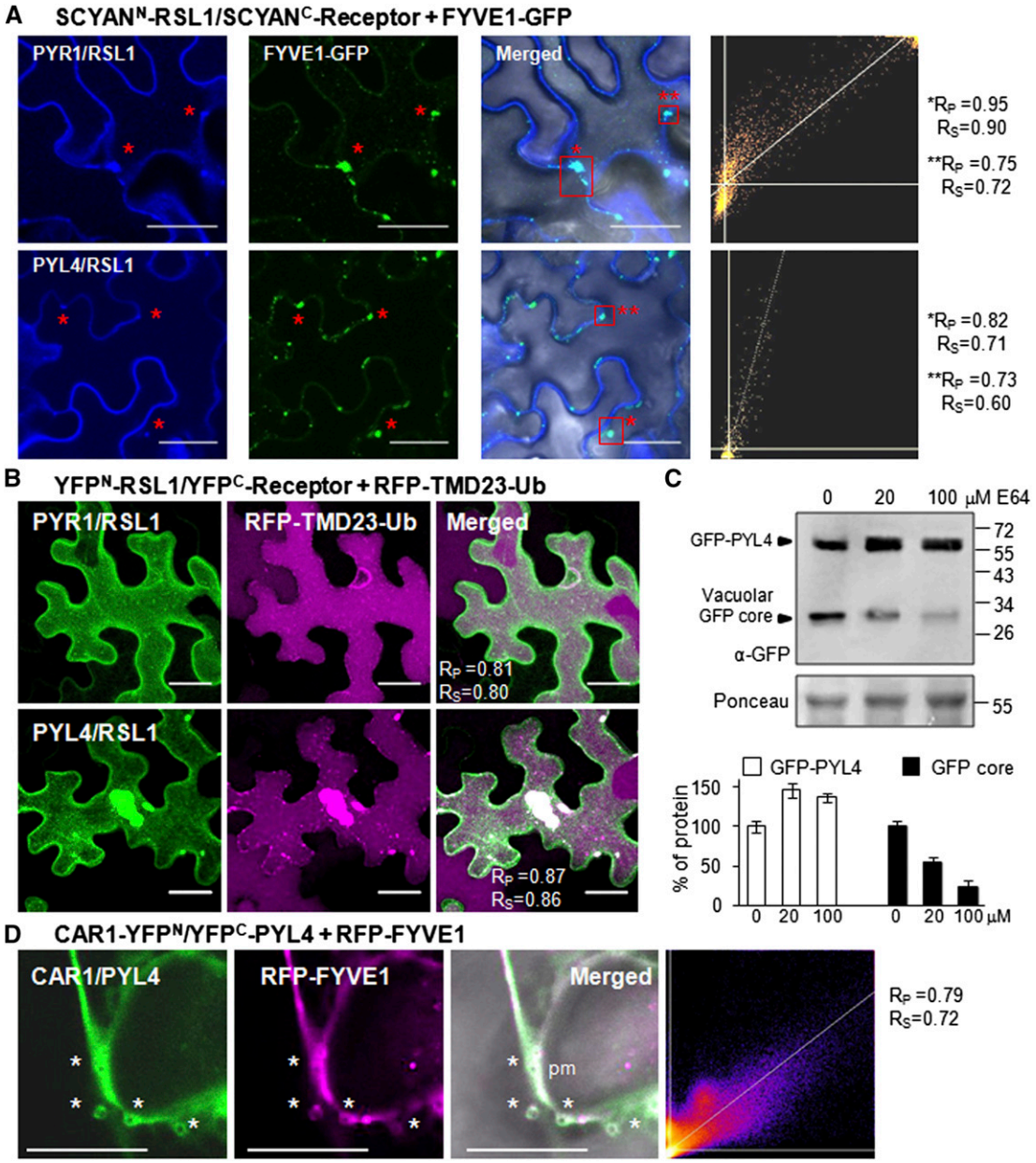

Figure 2. Coexpression of Receptor-RSL1 Complexes with the Vacuolar Marker RFP-TMD23-Ub Reveals Transit of PYR1/PYL4 ABA Receptors to the Vacuole.

(A) Colocalization of Receptor-RSL1 complexes with FYVE1. Epifluorescence confocal images were obtained 48 h after Agroinfiltration of tobacco epidermal cells with constructs encoding SCYAN^N-RSL1 and SCYAN^C-PYR1 or PYL4 plus FYVE1-GFP. Levels of colocalization for red boxed regions ($n > 20$) are depicted in relative intensity (*x*-, *y* axes) scatterplots. Values of Rp and Rs coefficients were calculated and are given next to scatterplots. Rp and Rs coefficients were greater than 0.6 for the endocytic vesicles analyzed. Bars = 30 μm.

(B) Coexpression of Receptor-RSL1 complexes with the vacuolar marker RFP-TMD23-Ub. CLSM 3D projection through a full *z*-series of confocal images obtained 72 h after Agroinfiltration of tobacco epidermal cells with constructs encoding YFP^N-RSL1 and YFP^C-PYR1 or PYL4 plus RFP-TMD23-Ub. Plants were incubated in darkness for 4 h in order to promote stabilization of the fluorescent protein-tagged vacuolar marker and RSL1-receptor complexes. Bars = 30 μm.

(C) Immunoblot analysis to monitor vacuolar delivery of GFP-PYL4. Seedlings expressing GFP-PYL4 were either mock- or E64-treated for 4 h. Protein extracts were analyzed by immunoblot using an anti-GFP antibody (upper panel) and Ponceau staining (middle panel) and were then quantified using Image Guache V4.0 software (lower panel). Bars show mean protein levels normalized to Rubisco protein. Values are averages ± SE of three independent experiments.

reminiscent of MVBs (Figure 3A). By contrast, FYVE1 did not interact with TOL4 or TOL9 proteins (Figures 1C and 3A), which are defined as gatekeepers for sorting of ubiquitylated cargo to the vacuole and whose modular domain structure shows similarity to ESCRT-0 proteins (Korbei et al., 2013). Immunoblot analysis verified the expression of each fusion protein in BiFC experiments (Figure 3B).

We also investigated the interaction of Snf7 with FYVE1 via cotransformation of BY-2 cells using biolistic bombardment. Following coexpression of GFP-FYVE1 and RFP-Snf7A, we observed colocalization in endosomal membranes (LEs/MVBs) (Figure 3C). Consistent with previous results, FYVE1 and Vps23 also colocalized in BY-2 cells and, hence, served as a positive control (Figure 3D). By contrast, FYVE1 did not colocalize with TOL4 or TOL9 proteins (Figure 3D). Snf7A expressed individually in BY-2 cells localized to large, globular-shaped structures that were previously identified as endosomal/MVBs through coexpression with the marker Syp21 (Richardson et al., 2011). These structures were also visualized through coexpression of GFP-FYVE1 and RFP-ARA7 in BY-2 cells, in which GFP-FYVE1 localized to both punctuate and globular RFP-ARA7-containing LEs (Supplemental Figure 4B). The globular-shaped LEs were far more prevalent in cells at later time points following biolistic bombardment and, hence, were likely due to the aggregation of the organelles in these cells, as reported elsewhere (Richardson et al., 2011).

Taken together, these results suggest that FYVE1 can bridge ESCRT-I and ESCRT-III complexes via its interaction with Vps23A and Snf7A. Recent structural studies of the ESCRT system in yeast support a close association of ESCRT-I and -III complexes (Williams and Urbé, 2007; Peel et al., 2011). Several viruses are able to bridge ESCRT complexes, including complexes I and III (Martin-Serrano et al., 2003; Strack et al., 2003; Richardson et al., 2014). Indeed, it was suggested that the ESCRT-III regulator ALIX/Bro1 might establish a link between ESCRT-I and -III, as it interacts with both Snf7/CHMP4 through its Bro1 domain and with TSG101 (mammalian ortholog of yeast Vps23) through a PTAP motif in the C-terminal region of ALIX (Martin-Serrano et al., 2003; Strack et al., 2003; Odorizzi, 2006). Likewise, the observed interaction of FYVE1 with Vps23A and Snf7A might bridge both complexes.

PYL4 Can Be Localized in Endosomal Compartments

Initial studies on the subcellular location of PYR/PYL receptors pointed out to cytosolic and nuclear localization of them (Ma et al., 2009; Park et al., 2009; Santiago et al., 2009). This point of view is complemented by recent work that supports membrane localization as peripheral proteins for a fraction of the total receptor pool (Demir et al., 2013; Jones et al., 2014; Bueso et al., 2014; Rodriguez et al., 2014; Diaz et al., 2016). For instance, the interaction of ABA receptors with RSL1 occurs at the plasma membrane (Bueso et al., 2014), and the study of CAR proteins reveals that perception of ABA at the plasma membrane affects ABA signaling (Rodriguez et al., 2014; Diaz et al., 2016). To further investigate the subcellular localization of PYL4, we expressed GFP-PYL4 in living tobacco cells and performed live-cell imaging using CLSM (Figure 4A; Supplemental Movie 1). GFP-PYL4 was localized mostly in the nucleus and the cytosol. However, we also found a minor portion of GFP-PYL4 in small endosomal vesicles in plants that were transferred from light to dark for 1 d (Figure 4A; Supplemental Movie 1). It was reported that, under acidic pH, the light-induced conformational change in GFP leads to the disappearance of GFP fluorescence in vacuoles; therefore, by transferring the plants from the light to the dark, it is possible to visualize vacuolar-targeted GFP (Tamura et al., 2003). Coexpression of FYVE1-GFP and RFP-PYL4 also revealed the presence of PYL4 in endosomal compartments and partial colocalization of FYVE1 and PYL4 in them (Figure 4B; Supplemental Movie 2).

To further analyze PYL4 endosomal trafficking, we generated Arabidopsis lines that express GFP-PYL4 and then used CLSM to visualize its subcellular localization in root cells in response to different pharmacological treatments. Under mock conditions, GFP-PYL4 was localized mostly to nucleus and cytosol (Figure 4C, see below), as described for PYR/PYLs (Santiago et al., 2009; Ma et al., 2009). BFA is a fungal toxin known to inhibit a GTP exchange factor for ARF GTPases (ARF-GEF) that is crucial for exocytosis. Therefore, this drug prevents recycling of endosomes and leads to accumulation of cargo in BFA-induced compartments (Dhonukshe et al., 2007; Robinson et al., 2008). After BFA treatment for 1 h, we found that GFP-PYL4 accumulated in BFA bodies of root cells, and the endosomal origin of the observed BFA bodies was confirmed by FM4-64 staining because this dye is an endocytic tracer (Vida and Emr, 1995) (Figure 4C, upper panels). Washing out the drug for 2 h allows the recovery of the wild-type cellular phenotype and redistributes GFP-PYL4, which appears localized mostly in the nucleus and the cytosol (Figure 4C, lower panels). Similar results were obtained after BFA treatment of Arabidopsis seedlings expressing GFP-PYL5 or GFP-PYL6, indicating that PYL4/5/6 receptors can be localized in endosomal compartments (Supplemental Figures 5A and 6A).

To further illustrate the presence of GFP-PYL4 in endosomal compartments, we obtained Arabidopsis plants expressing both GFP-PYL4 and the mCherry-ARA7 marker. CLSM imaging and quantification of signals from GFP and mCherry channels did not show significant overlap in mock conditions, as expected. However, when seedlings were treated with wortmannin (WM), a PI3K-inhibitor that inhibits protein cargo trafficking to vacuoles and causes enlargement of MVBs (Robinson et al., 2008), statistical

Figure 2. (continued).

(D) Interaction of PYL4 and CAR1 generates punctate/globular structures in plasma membrane and cytosol that colocalize with RFP-FYVE1. Photographs show epifluorescence confocal images of transiently transformed tobacco epidermal cells coexpressing CAR1-YFP^N/YFP^C-PYL4 interacting proteins and RFP-FYVE1. Asterisks indicate the presence of CAR1-PYL4 in membrane complexes that colocalize with FYVE1. Levels of colocalization for regions labeled with an asterisk are depicted in relative intensity (*x*-, *y* axes) scatterplots. Values of Rp and Rs coefficients were calculated and are given next to scatterplots. pm, plasma membrane. Bars = 30 μm.

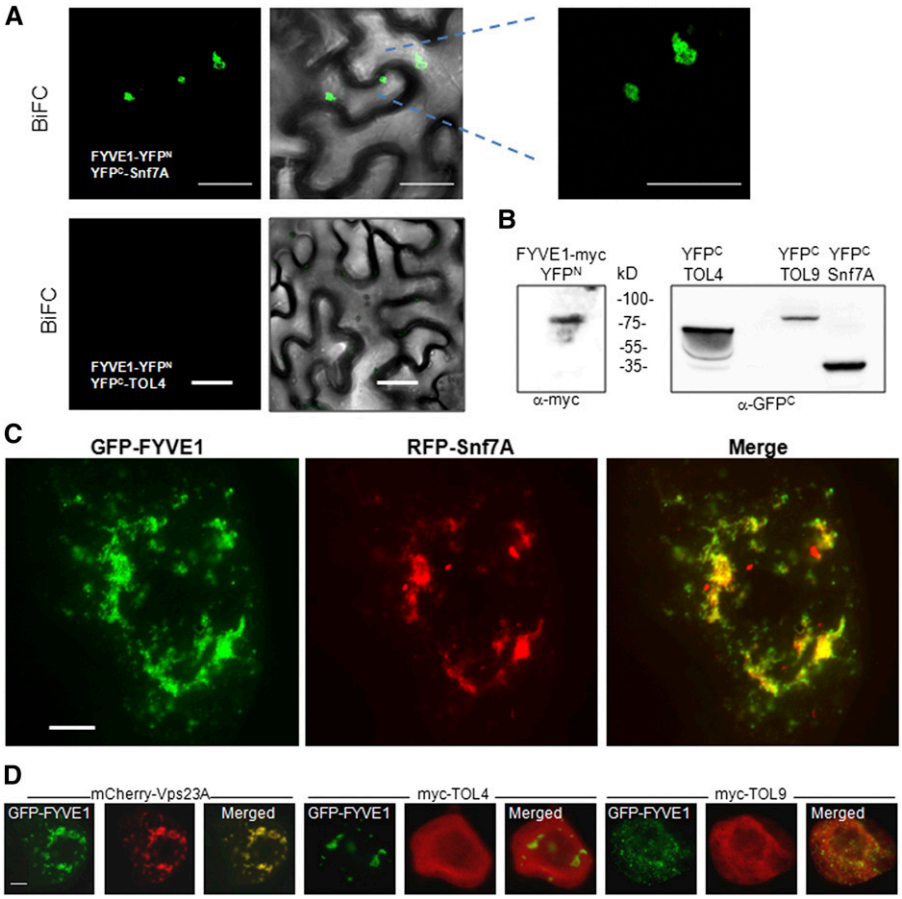

Figure 3. BiFC Interaction of FYVE1-YFP^N with YFP^C-SNF7A Labels Globular-Shaped Structures Representing LEs/MVBs.

(A) Epifluorescence confocal images of transiently transformed tobacco epidermal cells coexpressing FYVE1-YFP^N and YFP^C-Snf7A. The right panel shows a detail of the BiFC fluorescent signal. FYVE1-YFP^N does not interact with YFP^C-TOL4 in a BiFC assay. Bars = 20 μm.

(B) Immunoblot analyses of protein extracts (20 μg of total protein) obtained from tobacco leaves infiltrated with the indicated constructs and revealed using anti-myc or anti-GFP^C antibodies.

(C) Colocalization of GFP-FYVE1 and RFP-Snf7A (r = 0.64). BY-2 cells were cotransformed with GFP-FYVE1 and RFP-Snf7A gene constructs and the cells were processed, imaged, and analyzed by CLSM as described in Methods. Bar = 10 μm.

(D) Cotransformation of GFP-FYVE1 and mCherry-Vps23A reveals colocalization in LEs/MVBs (r = 0.74). By contrast, GFP-FYVE1 and myc-TOL proteins do not colocalize significantly (r = 0.3). Bar = 10 μm.

analysis (Pearson and Spearman's correlation coefficients) indicated colocalization of GFP-PYL4 and mCherry-ARA7 in WM-induced compartments (Figure 4D). The nature of these compartments was investigated using LysoTrackerRed, an acidophilic probe that labels lytic compartments in the late endocytic pathway (Nodzynski et al., 2013). As shown in Supplemental Figure 5B, late endocytic vesicles (MVBs/PVCs) decorated by LysoTrackerRed contained GFP-PYL4. Altogether, these results suggest that a fraction of the total PYL4 pool follows endocytosis and trafficking to the vacuole. Additionally, WM treatment of Arabidopsis plants expressing GFP-PYL5 or GFP-PYL6 also revealed the presence of this ABA receptor in compartments that were stained with LysoTrackerRed (Supplemental Figures 5C and 6B). Finally, treatment with concanamycin A, a specific vacuolar H-ATPase inhibitor that blocks protein degradation at the vacuole (Pali et al., 2004), revealed the presence of GFP-PYL5 in the vacuolar lumen of root epidermal cells (Supplemental Figure 5C). Altogether, these results suggest that ABA receptors follow endosomal trafficking and are delivered to the vacuole.

Clathrin-Mediated Endocytosis of ABA Receptors

Data from this study indicate that ABA receptors follow endocytic turnover from the plasma membrane to the vacuole. To further investigate this process, we performed proteomic analysis of immunocomplexes obtained from plants expressing HA-tagged PYR1, PYL4, or PYL8 that were treated with MG132. Proteasome activity has been shown to interfere with plasma membrane protein degradation and MG132 treatment stabilizes membrane proteins that undergo ubiquitylation and endocytosis (Abas et al., 2006; Göhre et al., 2008; Lee et al., 2009a). Protein extracts were immunopurified with anti-HA-coated magnetic beads and

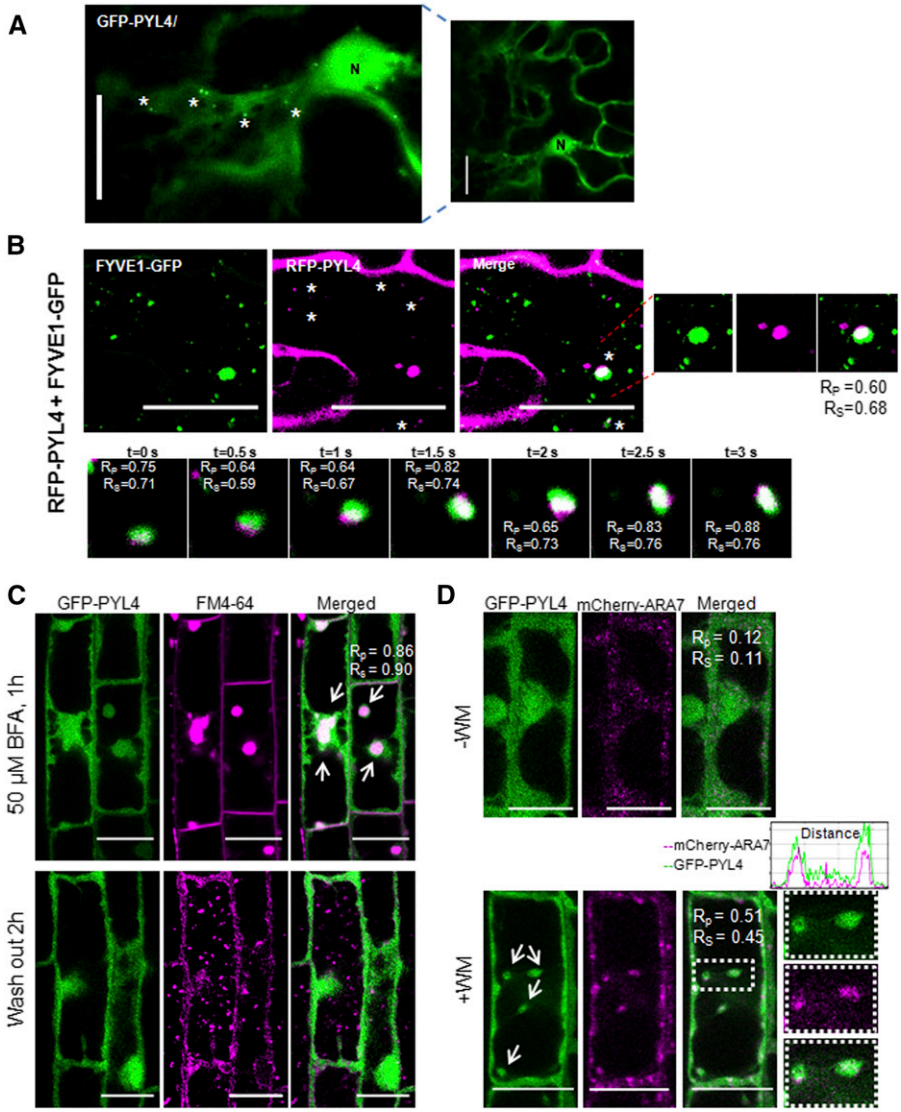

Figure 4. Localization of PYL4 in Endosomal Compartments.

(A) GFP-PYL4 is localized mostly in the nucleus (N) and cytosol of tobacco leaf cells after Agroinfiltration. A minor fraction of GFP-PYL4 decorates endosomal vesicles (asterisks) in 1-d dark-adapted tobacco plants. Bars = 30 μm

(B) Epifluorescence confocal images of transiently transformed tobacco epidermal cells coexpressing FYVE1-GFP and RFP-PYL4 (upper panels). Time-course photographs show comigration of RFP-PYL4 and FYVE1-GFP in endosomal compartments (lower panels). Bars = 15 μm.

(C) GFP-PYL4 accumulates in BFA compartments and shows colocalization with the endocytic marker FM4-64. Rp and Rs coefficients were greater than 0.7 for the BFA bodies analyzed ($n > 20$) by CLSM of root epidermal cells from Arabidopsis transgenic lines expressing GFP-PYL4. Four-day-old seedlings were labeled with 4 μM FM4-64 for 10 min, followed by 50 μM BFA treatment for 1 h. After washing in MS medium for 2 h, GFP-PYL4 redistributes and appears localized mostly in the nucleus and cytosol. Arrows mark BFA bodies. Bars = 10 μm.

(D) Colocalization of GFP-PYL4 and mCherry-ARA7 in WM-induced compartments. CLSM of root epidermal cells from seedlings coexpressing GFP-PYL4 and the LE-marker mCherry-ARA7 were analyzed after either a mock or a 33 μM WM treatment for 1 h. The 5× enlarged images (dotted boxes) were used for statistical analysis of GFP-PYL4 and mCherry-ARA7 colocalization in WM compartments. The intensity profiles of GFP (green) and mCherry (magenta) fluorescence were measured along the indicated distance (microns). Bars = 10 μm.

analyzed by LC-MS/MS. We found that components of the clathrin-dependent coating and scission machinery coimmunoprecipitated with HA-tagged PYR/PYL ABA receptors (Table 2). Proteomics data have been deposited to the ProteomeXchange Consortium (Vizcaíno et al., 2014). We found clathrin heavy chain (CHC)/clathrin light chain (CLC) subunits and different dynamin-related proteins that coimmunoprecipitated with HA-PYR1, HA-PYL4, and HA-PYL8 but were absent in samples obtained after immunoprecipitation of protein extracts expressing only the triple HA epitope (Table 2).

Clathrin-coated vesicles require adaptor proteins (APs) as co-coatomers and a large number of APs for clathrin have been characterized in plants (Paez Valencia et al., 2016). Interestingly, among the coimmunoprecipitated proteins, we also found components of the heterotetrameric AP-2 complex, which is involved in endocytosis of cargo proteins such as BRI1 from the plasma membrane (Chen et al., 2011; Di Rubbo et al., 2013). Moreover, we found some components of the TPLATE adaptor complex, which is recruited at the plasma membrane preceding recruitment of the AP-2 complex, clathrin, and dynamin-related proteins (Gadeyne et al., 2014). To further validate the above data, we performed immunoprecipitation (IP) of CHC from plants expressing HA-PYL4 using the α-CHC1,2 antibody (Agrisera 10690) and we tested the coIP of HA-PYL4 using α-HA antibody. We found that HA-PYL4 coimmunoprecipitated with CHC, but incubation with Tyrphostin A23 (TyrA23), a known inhibitor of clathrin-mediated endocytosis (Dhonukshe et al., 2007), abolished coimmunoprecipitation of HA-PYL4 with CHC (Figure 5A). To obtain additional evidence, we coexpressed CLC-mOrange (driven by its own promoter; Konopka et al., 2008) and GFP-PYL4 proteins in tobacco cells and found they colocalized in endocytic vesicles near the plasma membrane (Figure 5B). Altogether, these results suggest that ABA receptors follow endocytosis through clathrin-coated vesicles.

Knockdown fyve1 Alleles Show Enhanced Sensitivity to ABA and Defects in Vacuolar Morphology

Although 15 FYVE domain-containing proteins have been identified in the Arabidopsis genome, a BLAST search indicated that there are no close homologs to FYVE1 (Gao et al., 2014). FYVE1 is presumed to play an essential role in plant cell viability because homozygous knockout *fyve1-1/free1* and *fyve1-2* alleles are seedling lethal (Barberon et al., 2014; Gao et al., 2014; Kolb et al., 2015). In order to investigate the biological relevance of FYVE1 function in the context of ABA signaling, we screened the ABRC/NASC T-DNA insertion collection for *fyve1* alleles that are expected to retain some function (Supplemental Figure 7). Two viable hypomorphic *fyve1* alleles were recovered from the ABRC/NASC collection. The *fyve1-3* allele bears a T-DNA insertion in the FYVE1 promoter, ~150 nucleotides upstream of the ATG start codon, and although qRT-PCR analysis showed diminished expression of *FYVE1* in *fyve1-3*, it retained ~50% of wild-type expression (Supplemental Figure 7). The *fyve1-4* allele bears a T-DNA insertion in the last intron of the gene, disrupting production of full-length *FYVE1* mRNA (Supplemental Figure 7). Both alleles showed enhanced sensitivity to 0.5 μM ABA-mediated inhibition of seedling establishment (Figure 6A), indicating that diminished expression of *FYVE1* leads to enhanced response to ABA. As a reference for the ABA-hypersensitive phenotype, we used the *hab1-1abi1-2* double mutant, which lacks the HAB1 and ABI1 negative regulators of ABA signaling and showed enhanced sensitivity to ABA (Saez et al., 2006). Finally, heterozygous (+/−) *fyve1-1* seeds are viable and able to germinate, but they showed enhanced sensitivity to ABA-mediated inhibition of seedling establishment and shoot growth compared with the wild type (Figure 6B). This result also indicates that *FYVE1* gene dosage affects ABA sensitivity since (+/−) *fyve1-1* plants do have altered response to ABA compared with the wild type.

We scored ABA-mediated root growth inhibition of homozygous *fyve1-3* and (+/−) *fyve1-1* seedlings (genotype *a posteriori*), and we observed enhanced ABA sensitivity in these mutants compared with the wild type (Figure 6C). Analysis of radical emergence in plates supplemented with 0.5 μM ABA indicated that both *fyve1-3* and (+/−) *fyve1-1* seed progeny were hypersensitive to ABA-mediated inhibition of seed germination (Figure 6D). Expression of ABA-responsive genes was analyzed in *fyve1-3* and (+/−) *fyve1-1* seedlings compared with the wild type, and we found that *RAB18* and *RD29B* were upregulated by endogenous ABA in plants with *fyve1* alleles (Figure 6E). Because ABA plays a critical role in regulating stomatal aperture and water loss, water-loss assays were performed using 15-d-old seedlings. We found that *fyve1-3* showed reduced water loss compared with the wild type (Figure 6F). Therefore, because reduced FYVE1 function leads to ABA hypersensitivity, FYVE1 appears to play a negative role in ABA signaling.

FYVE1 plays a key role for intracellular trafficking processes and null *fyve1-1* and *fyve1-2* alleles display a prominent defect in endocytic trafficking and vacuole biogenesis (Gao et al., 2015; Kolb et al., 2015). Endocytic trafficking events can be monitored using the endocytic tracer dye FM4-64 (Vida and Emr, 1995; Jelínková et al., 2010). We examined root meristem cells of wild-type, (+/−) *fyve1-1*, *fyve1-3*, and *fyve1-4* plants using CLSM following staining with FM4-64 for 3 h, which labels late endocytic compartments (Supplemental Figure 8A). Aberrant endomembrane structures were observed in *fyve1* mutants, which likely reflect the altered vacuolar morphology described previously in *fyve1-1* (Kolb et al., 2015). Staining of epidermal cells in cotyledons also revealed a clear defect in the vacuolar structure of *fyve1-1* cells, whereas small endomembranes were apparent in *fyve1-3* and *fyve1-4* cells that were not found in the wild type (Supplemental Figure 8A). To further establish the vacuolar phenotype of plants containing knockdown *fyve1* alleles, we used the 2′,7′-bis-(2-carboxyethyl)-5-(and-6)-carboxyfluorescein)-acetoxymethyl ester (BCECF-AM) probe, which labels acidic compartments such as the vacuole, followed by CLSM visualization. Vacuoles of (+/−) *fyve1-1*, *fyve1-3*, and *fyve1-4* plants were altered compared with the wild type (Supplemental Figure 8B). A three-dimensional reconstruction analysis by surface rendering on Z-stack images was performed for vacuoles of wild-type, (+/−) *fyve1-1*, *fyve1-3*, and *fyve1-4* plants. As a result, we observed altered vacuolar morphology in plants with knockdown *fyve1* alleles, and these plants contained tubular structures that were absent in wild-type plants.

fyve1 Mutants Show Enhanced Accumulation of Ubiquitylated PYL4

To further study the role of FYVE1 in PYL4 endosomal trafficking, we generated double transgenic lines that express GFP-PYL4 or HA-PYL4 in the *fyve1-3* background. In root epidermal cells of *fyve1-3* plants, but not in wild-type plants, we found that GFP-PYL4 accumulated in endocytic vesicles stained with FM4-64 (Figure 7A). Seedlings were treated with WM and in wild-type plants we detected late endocytic vesicles decorated by LysoTrackerRed that contained GFP-PYL4. By contrast, GFP-PYL4 did not reach these enlarged MVBs/PVCs in *fyve1-3* cells,

Table 2. Coimmunoprecipitated Proteins after IP of HA-Tagged ABA Receptors

	Identified Proteins					
IP Protein	Locus	Name	Score	Sequence Coverage	Unique Peptides	MM (kD)
PYR1	At4g17870	Abscisic acid receptor PYR1	135.64	84.29	16	21.56
	At1g23900	AP-1 complex subunit gamma-1	16.06	48.63	6	96.41
	At1g60070	AP-1 complex subunit gamma-2	7.81	49.65	13	94.61
	At2g17380	AP-1 complex subunit sigma-1	1.65	50.93	2	18.75
	At5g22770	AP-2 complex subunit alpha-1	20.02	55.43	12	112.08
	At1g31730	AP-4 complex subunit epsilon	21.00	46.06	17	103.67
	At3g11130	Clathrin heavy chain 1	98.43	51.67	4	193.12
	At3g08530	Clathrin heavy chain 2	105.14	52.55	7	193.15
	At2g20760	Clathrin light chain 1	24.14	58.88	8	37.20
	At2g40060	Clathrin light chain 2	13.29	63.18	5	28.82
	At5g42080	DRP1A	4.96	69.67	6	68.13
	At1g10290	DRP2A	16.50	52.95	4	99.11
	At1g59610	DRP2B	23.79	53.04	8	100.17
	At4g32285	Clathrin assembly protein CAP1	17.35	59.53	12	70.51
	At3g01780	Protein TPLATE	21.43	44.47	5	130.83
	At5g45750	Ras-related protein RABA1c	11.98	64.81	2	23.86
	At1g09630	Ras-related protein RABA2a	12.06	68.66	2	24.09
	At2g43130	Ras-related protein RABA5c	10.47	45.33	1	23.97
	At5g47200	Ras-related protein RABD2b	7.31	46.53	1	22.30
	At3g46060	Ras-related protein RABE1c	11.40	80.09	2	23.82
PYL4	At2g38310	Abscisic acid receptor PYL4	439.65	54.11	10	22.42
	At3g11130	Clathrin heavy chain 1	17.72	14.31	10	193.24
	At3g08530	Clathrin heavy chain 2	38.96	0.82	1	193.15
	At2g40060	Clathrin light chain 2	39.56	7.75	1	28.82
	At5g42080	DRP1A	2.32	7.21	1	68.13
	At1g14830	DRP1C	2.00	2.93	1	68.72
	At2g44590	DRP1D	29.59	1.51	1	66.58
	AT1G59610	DRP2B	7.64	16.09	5	100.17
	At4g17170	Ras-related protein RABB1c	2.08	11.37	1	23.16
	At5g47200	Ras-related protein RABD2b	6.00	34.65	3	22.30
	At3g53610	Ras-related protein RABE1a	2.00	20.37	2	23.94
	At3g46060	Ras-related protein RABE1c	2.17	25.46	2	23.82
PYL8	At5g53160	Abscisic acid receptor PYL8	27.38	81.91	7	21.38
	At1g23900	AP-1 complex subunit gamma-1	29.00	39.95	11	96.41
	At1g60070	AP-1 complex subunit gamma-2	43.80	48.38	17	94.61
	At2g17380	AP-1 complex subunit sigma-1	15.89	80.12	8	18.75
	At5g22770	AP-2 complex subunit alpha-1	59.82	51.09	28	112.08
	At1g31730	AP-4 complex subunit epsilon	59.09	60.13	19	103.67
	At3g11130	Clathrin heavy chain 1	209.41	51.20	5	193.12
	At3g08530	Clathrin heavy chain 2	216.50	53.85	9	193.15
	At2g20760	Clathrin light chain 1	65.13	60.95	14	37.20
	At2g40060	Clathrin light chain 2	40.26	63.18	12	28.82
	At5g42080	DRP1A	55.37	72.95	20	68.13
	At1g10290	DRP2A	61.47	61.82	5	99.11
	At1g59610	DRP2B	61.70	61.30	7	100.17
	At3g01780	Protein TPLATE	50.23	54.68	22	130.83
	At5g45750	Ras-related protein RABA1c	10.91	64.81	1	23.86
	At1g09630	Ras-related protein RABA2a	18.93	70.51	2	24.09
	At3g46830	Ras-related protein RABA2c	11.29	57.14	1	23.83
	At5g47200	Ras-related protein RABD2b	19.85	75.74	1	22.30
	At3g46060	Ras-related protein RABE1c	20.79	89.35	6	23.82

LC-MS/MS proteomic analyses of coimmunoprecipitated proteins after IP of either HA-tagged PYR1, PYL4, or PYL8 receptors was performed as reported (Castillo et al., 2015). The MS proteomics data have been deposited to the ProteomeXchange Consortium (Vizcaíno et al., 2014) through the PRIDE partner repository with the data set identifiers PXD002396 and 10.6019/PXD002396. MM, molecular mass.

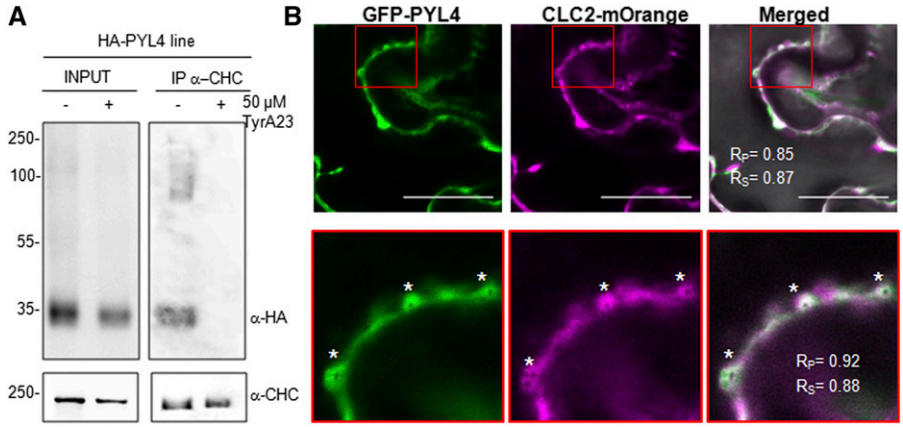

Figure 5. Clathrin-Mediated Endocytosis of PYL4.

(A) Coimmunoprecipitation of HA-PYL4 with CHC protein is inhibited by TyrA23. Anti-CHC1,2 antibody (Agrisera 10690) was used to immunoprecipitate CHC from Arabidopsis protein extracts (1 mg of total protein each) prepared from plants expressing 3HA-PYL4. Protein extracts were prepared from plants that were treated with 50 μM MG132 or 50 μM MG132+50 μM TyrA23 for 6 h. Input levels of CHC and HA-PYL4 in crude protein extracts (20 μg of total protein) were analyzed by immunoblotting. Immunoprecipitated CHC protein was probed with anti HA-HRP antibody to detect coimmunoprecipitation of PYL4.

(B) Colocalization of GFP-PYL4 with CLC2-mOrange in clathrin-coated vesicles at the plasma membrane. Epifluorescence confocal images were obtained 48 h after agroinfiltration of tobacco epidermal cells with constructs encoding GFP-PYL4 and CLC2-mOrange (Konopka et al., 2008). Pearson's and Spearman's correlation coefficients indicate colocalization of PYL4 and CLC2. Bars = 20 μm.

suggesting that reduced FYVE1 function in *fyve1-3* leads to a blockade of GFP-PYL4 targeting to MVBs/PVCs and the vacuole (Figure 7B).

These results are in agreement with the lack of vacuolar accumulation of PIN2-GFP in FREE1 RNAi plants (Gao et al., 2014). Indeed, FREE1 function in the ESCRT pathway involves the sorting of cargoes into the ILVs of MVBs and ultimate releasing them into the vacuolar lumen (Gao et al., 2014). Taken together, the experiments described in this study suggest that ABA receptors follow endocytosis and that FYVE1 mediates delivery of ubiquitylated PYL4 to the ESCRT machinery for subsequent vacuolar degradation. Therefore, the impairment of FYVE1 function should lead to reduced degradation of PYL4 and accumulation of ubiquitylated PYL4. Indeed we found that protein level of HA-PYL4 was higher in *fyve1-3* plants than in wild-type plants (Figure 7C), whereas the *HA-PYL4* transcript level was not significantly different (Supplemental Figure 9A). Additionally, enhanced accumulation of ubiquitylated proteins was observed for *fyve1-3* compared with the wild type, confirming previous results from Gao et al. (2014) using an RNAi approach against FYVE1 under the control of a dexamethasone (DEX)-inducible system (FREE1 DEX-RNAi) and Kolb et al. (2015) using *fyve1-2*. As a second source of evidence, we examined protein levels of GFP-PYL4 in FREE1 DEX-RNAi plants with and without DEX induction. CLSM imaging of GFP-PYL4 revealed higher fluorescence after DEX treatment compared with mock treatment (Supplemental Figure 9B), suggesting enhanced accumulation of GFP-PYL4. This was verified by immunoblot analysis using anti-GFP and anti-FREE1 antibodies to confirm the successful induction of the FREE1 silencing system (Figure 7D). The transcript level of *GFP-PYL4* was not significantly altered by DEX treatment (Supplemental Figure 9A). Therefore, both *fyve1-3* and induced FREE1 DEX-RNAi plants accumulated higher levels of PYL4 without affecting *PYL4* mRNA accumulation (Figures 7C and 7D).

Impairment of FYVE1 function might lead to enhanced accumulation of ubiquitylated ABA receptors. To test this possibility, we prepared protein extracts from HA-PYL4 *fyve1-3* lines and purified ubiquitylated proteins using p62-agarose affinity purification, which exploits the Ub-interacting motif of the mammalian p62 protein. Next, we probed with anti-HA to detect ubiquitylated HA-PYL4. As a result, we found enhanced accumulation of monoubiquitylated HA-PYL4 in *fyve1-3* plants compared with wild-type plants (Figure 7C, right panel). Finally, in FREE1 DEX-RNAi lines without and with DEX induction, we immunoprecipitated GFP-PYL4, and after immunoblot analysis using anti-Ub, we could detect enhanced accumulation of ubiquitylated GFP-PYL4 (Figure 7D, right panel). Overall, our results suggest that *fyve1* alleles diminish vacuolar degradation of ABA receptors and lead to enhanced accumulation of ubiquitylated receptors.

DISCUSSION

Ubiquitylation of integral membrane proteins is critical for endosomal sorting and vacuolar targeting (Barberon et al., 2011; Kasai et al., 2011; Leitner et al., 2012; Martins et al., 2015). A common step in the vacuolar degradation pathway of membrane proteins is ESCRT-mediated sorting for delivery into ILVs of MVBs (Raiborg and Stenmark, 2009). The ESCRT pathway has been assumed to be reserved for integral membrane proteins, as exemplified by plant cell surface proteins such as BOR1, PIN2, BRI1, IRT1, or PHT1 (Spitzer et al., 2009; Kasai et al., 2011; Leitner et al., 2012; Martins et al., 2015; Barberon et al., 2011; Cardona-López et al., 2015). However, in this work, we showed the involvement of the

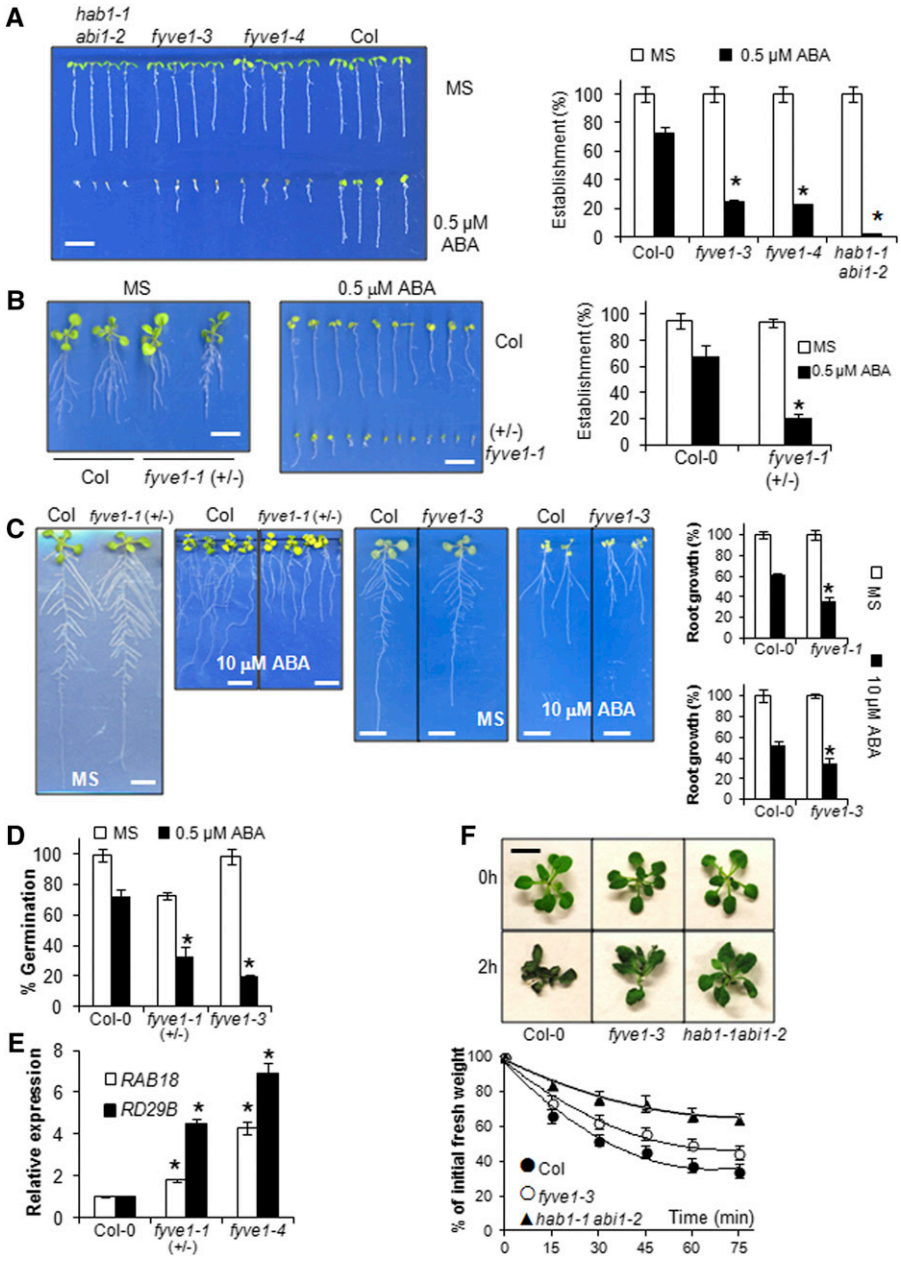

Figure 6. Reduction-of-Function *fyve1* Alleles Cause Enhanced Sensitivity to ABA.

(A) Photographs of Col wild type, *fyve1-3*/*fyve1-4* alleles, and the *hab1-1abi1-2* ABA-hypersensitive mutant grown for 7 d on MS medium either lacking or supplemented with 0.5 μM ABA (left panel) and quantification of ABA-mediated inhibition of seedling establishment in the indicated backgrounds (right panel). Values are averages ± SE of three independent experiments ($n > 100$). Asterisk indicates $P < 0.05$ (Student's *t* test) compared with the wild type in the same assay conditions. Bar = 1 cm.

(B) Heterozygous *fyve1-1* seedlings show enhanced ABA-mediated inhibition of seedling establishment and growth compared with the wild type. Photographs of Col wild-type and *fyve1-1* plants grown for 13 d on MS medium either lacking (left panel) or supplemented with 0.5 μM ABA (middle panel). Quantification of seedling establishment at 7 d (right panel). Values are averages ± SE of three independent experiments ($n > 100$). Asterisk indicates $P < 0.05$ (Student's *t* test) compared with the wild type in the same assay conditions. Bars = 1 cm

(C) Enhanced ABA-mediated inhibition of root growth in (+/−) *fyve1-1* and *fyve1-3* mutants compared with Col wild type. Seedlings (5 d old) germinated on MS plates were transferred to new plates lacking or supplemented with 10 μM ABA. (+/−) *fyve1-1* seedlings were genotyped *a posteriori* (left and middle panels). Quantification of root growth after 10 d (right panels). Data are averages ± SE from three independent experiments ($n = 20$). Asterisk indicates $P < 0.05$ (Student's *t* test) compared with the wild type in the same assay conditions. Bars = 1 cm.

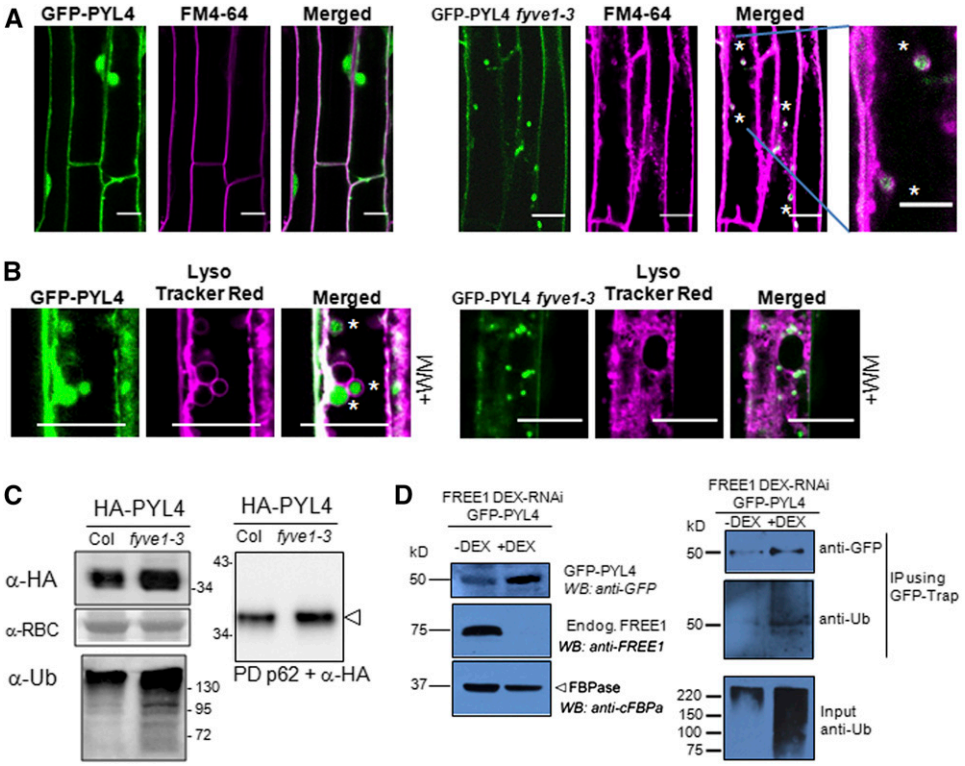

Figure 7. *fyve1* Mutants Show Enhanced Accumulation of Ubiquitylated PYL4.

(A) GFP-PYL4 decorates endocytic vesicles in *fyve1-3*. Asterisks (far right panels) indicate endocytic vesicles labeled by FM4-64 that contain GFP-PYL4. Epifluorescence confocal images of Arabidopsis root cells expressing GFP-PYL4 in wild-type or *fyve1-3* background stained with FM4-64. Bars = 15 μm.
(B) GFP-PYL4 is found in WM-induced rings of wild-type seedlings. Upon WM treatment, in wild-type seedlings GFP-PYL4 is observed in late endocytic vesicles decorated by LysoTrackerRed (indicated by asterisks), whereas GFP-PYL4 is absent from late endocytic compartments in *fyve1-3*. Bars = 20 μm.
(C) *fyve1-3* accumulates more PYL4 than the wild type and contains more ubiquitylated PYL4. Immunoblots with anti-HA, anti-RBC, and anti-ubiquitin P4D1 antibody from total protein extracts (left panel). Immunoblot with anti-HA antibody from ubiquitylated proteins pulled down using p62-agarose (right panel). Ubiquitylated HA-PYL4 was pulled down using p62-agarose from Col wild-type or *fyve1-3* protein extracts, and anti-HA immunoblotting was performed to detect HA-tagged ubiquitylated PYL4 (indicated by the open arrowhead).
(D) FREE1 DEX-RNAi plants induced with DEX accumulate more GFP-PYL4 than mock-treated plants and contain more ubiquitylated GFP-PYL4. Immunoblots with anti-GFP, anti-FREE1, and anti-FBP antibody from total protein extracts (left panel). Immunoblot analysis with anti-GFP and anti-Ub antibody from proteins that were immunoprecipitated using GFP-Trap (right panel).

ESCRT pathway in mediating the degradation of ABA receptors, which are not integral membrane proteins but can be found associated to membranes either through association with CAR proteins or via the single-subunit RING E3 ligase RSL1 (Bueso et al., 2014; Rodriguez et al., 2014; Diaz et al., 2016). In this work, we showed that RSL1-Receptor complexes can be a cargo for ESCRT to be delivered for vacuolar degradation. In agreement with this observation, the presence of RSL1 in early endosomes/trans-Golgi network and BFA compartments was documented previously (Bueso et al., 2014).

Figure 6. (continued).

(D) Enhanced ABA-mediated inhibition of seed germination in (+/−) *fyve1-1* seed progeny and the *fyve1-3* mutant compared with Col wild type. Values are averages ± SE of three independent experiments ($n > 100$). Asterisk indicates $P < 0.05$ (Student's *t* test) compared with the wild type in the same assay conditions.
(E) Enhanced expression of the ABA-responsive genes *RAB18* and *RD29B* in (+/−) *fyve1-1* seedlings and *fyve1-3* mutant compared with the Col wild type. mRNAs were prepared from 10-d-old seedlings of Col-0 wild type, *fyve1-1* heterozygous (+/−) individuals, and *fyve1-4* homozygous mutant and expression of *RAB18* and *RD29B* in response to endogenous ABA was quantified in real-time quantitative PCR experiments. Data are averages ± SE from three independent experiments ($n = 20$). Asterisk indicates $P < 0.05$ (Student's *t* test) compared with the wild-type in the same assay conditions.
(F) Diminished water loss in the *fyve1-3* mutant compared with Col wild type. Photographs show representative excised plants submitted for 2 h to the drying atmosphere of a flow laminar hood. Quantification of the loss of fresh weight in 15-d-old plants submitted to the drying atmosphere of a flow laminar hood. The graphic shows a polynomial fitting of the water loss kinetics. Data are averages ± SE from three independent experiments ($n = 5$). Bar = 1 cm.

Recently, mechanisms to regulate ABA signaling at a receptor protein level have been described, such as the nitric oxide-mediated inactivation of ABA receptors by tyrosine nitration and the proteasomal degradation of polyubiquitylated receptors (Irigoyen et al., 2014; Castillo et al., 2015). Additionally, the endosomal turnover of ubiquitylated PYR/PYL ABA receptors through the ESCRT pathway appears to be a novel route for modulation of ABA receptor function (Figure 8). The presence of ABA receptors associated with the plasma membrane is required for regulation of core ABA signaling components and key events in the ABA pathway (Demir et al., 2013; Brandt et al., 2015); therefore, a mechanism to regulate turnover of the receptors is likely important for regulation of these processes. For instance, clade A PP2Cs interact and dephosphorylate the slow anion channel SLAC1 and provide a mechanism ensuring specificity in Ca^{2+} signal transduction (Brandt et al., 2015). ABA receptors, through ABA-dependent inhibition of clade A PP2Cs, activate certain SnRK2s that are key regulators of different processes at the plasma membrane, such as the activation of the R- and S-type anion channels (Geiger et al., 2009; Lee et al., 2009b; Imes et al., 2013), the inhibition of K^+ uptake (Sato et al., 2009), the inhibition of H^+-ATPase (Merlot et al., 2007; Planes et al., 2015), the enhancement of water transport through certain aquaporins (Grondin et al., 2015), the endocytosis of the KAT1 K^+ channel (Sutter et al., 2007), or the activation of NADPH oxidases RbohF/D (Kwak et al., 2003; Sirichandra et al., 2009). ABA perception in the proximity of the plasma membrane also might facilitate the enhanced endocytosis of regions of the plasma membrane after osmotic stress through a rapid decrease in guard cell turgor pressure (Zwiewka et al., 2015). Therefore, regulation of ABA receptor turnover at the plasma membrane seems crucial for cellular homeostasis and stress response.

Previous reports have shown that FYVE1 plays a crucial role in mediating the delivery of ubiquitylated membrane proteins to ESCRT (Gao et al., 2014; Kolb et al., 2015). In addition to recognition of the ubiquitin moiety, it is possible that additional regions of the protein are involved in cargo recognition. Thus, our Y2H interaction assays suggest the N-terminal part of the protein, which contains an IDR, plays a critical role for recognition of ABA receptors. IDR regions adopt metastable conformations upon binding of interacting partners, and this allows molecular recognition of several targets with low affinity (Ward et al., 2004). Additionally, this region contains P(S/T)AP-like tetrapeptide motifs that are required for interaction with Vps23A (Gao et al., 2014). Therefore, the N terminus of FYVE1 is involved both in recognition of cargo and interaction with an ESCRT-I subunit. Vps23 (TSG101 in mammals) is a key subunit of ESCRT-I that has been reported to bind ubiquitin via the ubiquitin-conjugating E2

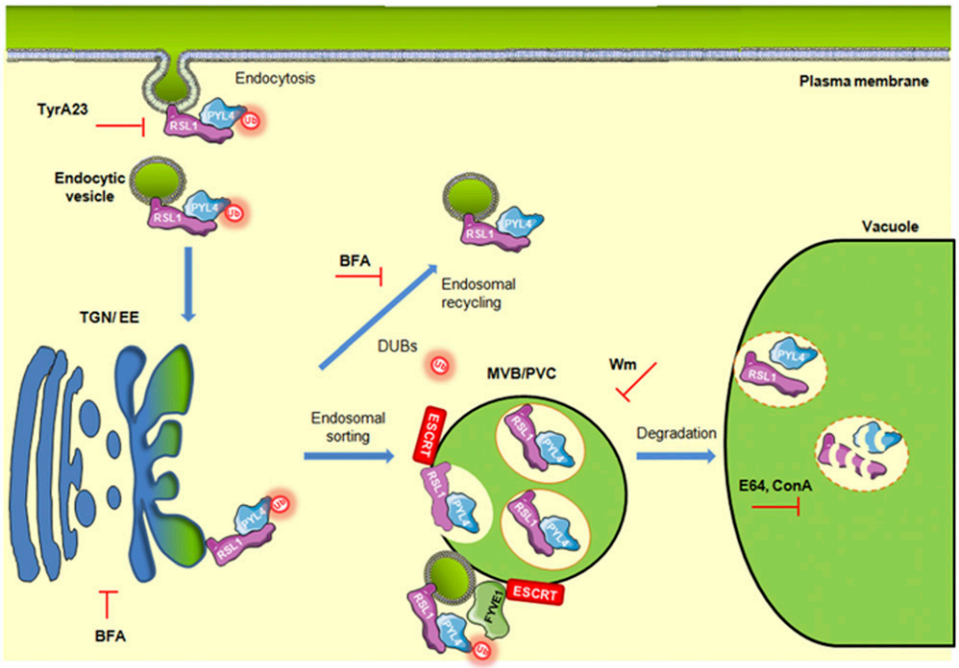

Figure 8. A Proposed Model of the Endosomal Trafficking of ABA Receptors and the Role of FYVE1 in Recruiting Ubiquitylated PYL4.

Ubiquitylation of PYL4 in the plasma membrane by RSL1 acts as a trigger for endocytosis. FYVE1 recognizes ubiquitylated PYL4 in the RSL1-PYL4 complex and recruits it to the ESCRT pathway, promoting degradative sorting of PYL4 at MVB/PVC. MVBs gain competence to fuse with the vacuole, where the RSL1-PYL4 complex is degraded. *fyve1* mutants are impaired in the targeting of PYL4 to the MVB/PVC for vacuolar degradation, which increases the half-life of PYL4 and leads to an enhanced response to ABA. Our model predicts that the ESCRT machinery is required for the turnover of ABA receptors; hence, additional ESCRT components participate in degradative sorting of ABA receptors. The possible participation of deubiquitinating enzymes (DUBs) in this pathway as well as the pharmacological interference with TyrA23, BFA, WM, E64, and ConA at different steps of endocytosis, endosomal trafficking, and vacuolar degradation is indicated.

enzyme variant (UEV) domain (Pornillos et al., 2002). Thus, Vps23 might cooperate with FYVE1 for binding of ubiquitylated cargo. The UEV domain in TSG101 binds not only to ubiquitylated cargo but also to P(S/T)AP motifs present in the C-terminal region of the ESCRT-III regulator ALIX (Pornillos et al., 2002; Martin-Serrano et al., 2003; Strack et al., 2003). Because we also found a connection of FYVE1 with the ESCRT-III subunit Snf7A, it is possible that both Vps23A and FYVE1 might bridge ESCRT-I and -III subcomplexes, as it has been previously suggested for ALIX (Odorizzi, 2006). Further studies are needed to fully elucidate the organization of the ESCRT machinery in plants.

Ubiquitylation serves as a signal for both endocytosis and sorting through the ESCRT machinery. The trafficking of ABA receptors from the plasma membrane to vacuole is likely dependent on their interaction with the E3 ligase RSL1, which ubiquitylates ABA receptors at the plasma membrane (Bueso et al., 2014). FYVE1 colocalized with RSL1-receptor complexes in the proximity of the plasma membrane (Figure 2) and FYVE1 binds directly to ubiquitin, which strongly suggests that FYVE1 carries ubiquitylated ABA receptors to the ESCRT machinery. Therefore, these data suggest that ubiquitylated cargos are captured by FYVE1 as a step for loading of the ESCRT machinery because orthologs of ESCRT-0 subunits are not found in higher plants (Raiborg and Stenmark, 2009; Richardson et al., 2011). Interestingly, Arabidopsis FYVE1, human (*Homo sapiens*) HRS, and yeast (*Saccharomyces cerevisiae*) Vps27 proteins all contain FYVE and Pro/Gln-rich domains and are able to bind ubiquitin. However, loading of the ESCRT machinery with ubiquitylated cargos also might be performed in plants by TOL proteins, but a full understanding of their connection with ESCRT complexes is still lacking (Korbei et al., 2013).

In mammalian cells, the human HRS protein recruits clathrin to early endosomes, providing a link between clathrin-mediated endocytosis and endosome sorting, and both HRS and the yeast ortholog Vps27 contain clathrin binding motifs (Raiborg et al., 2001, 2002). Clathrin-mediated endocytosis is the major mechanism for eukaryotic turnover of plasma membrane proteins (Chen et al., 2011; Gadeyne et al., 2014). After IP of HA-tagged PYR/PYL ABA receptors followed by LC-MS/MS analysis, we detected components of the clathrin-dependent coating and scission machinery that coimmunoprecipitated with ABA receptors. We also demonstrated both that PYL4 coimmunoprecipitated with CHC and that GFP-PYL4 colocalized with CLC in clathrin-coated vesicles near the plasma membrane (Figure 5), suggesting that ubiquitylated ABA receptors follow clathrin-mediated endocytosis. In agreement with this idea, BFA treatment revealed the presence of GFP-PYL4/PYL5/PYL6 in BFA bodies, suggesting that ABA receptors follow endosomal trafficking. Additional trafficking of ABA receptors was visualized through other pharmacological approaches. Although the subcellular location of PYL4 and ARA7 did not show significant overlap under mock conditions, when cargo trafficking to vacuole was inhibited using WM, we detected colocalization of PYL4 and ARA7 in endocytic compartments. Additionally, when vacuolar degradation was inhibited by Concanamycin A (ConA) treatment, PYL5 accumulated in the vacuole. Finally, we demonstrated that FYVE1 function is limiting for PYL trafficking. Thus, the *fyve1-3* mutant or FREE1 DEX-RNAi lines (induced with DEX) accumulated PYL4 to higher levels and contained more ubiquitylated receptor. Taken together, our data define a key role of FYVE1 in regulation of ABA receptor turnover from the plasma membrane and they reveal an unexpected mechanism for modulating ABA sensitivity through endosomal trafficking of ABA receptors. Interestingly, even heterozygous *fyve1-1* plants show an enhanced response to ABA, suggesting that *FYVE1* gene dosage is important for proper turnover of ABA receptors. Finally, given the reported interaction of FYVE1 with other ESCRT components, our work also predicts that other ESCRT subunits are required for the turnover of ABA receptors.

METHODS

Plant Material and Growth Conditions

Arabidopsis thaliana plants were grown as described by Pizzio et al. (2013). Knockdown insertion lines *fyve1-3* (SAIL_516_E05) and *fyve1-4* (SALK_205349) were obtained from the Nottingham Arabidopsis Stock Centre (http://nasc.nott.ac.uk). To confirm and identify homozygous T-DNA individuals, seedlings of each insertion line were grown individually and DNA from each plant was extracted and analyzed by PCR-mediated genotyping using the primers described in Supplemental Table 1. *fyve1-1/free1* (pst18264/15-1960 RIKEN BRC) was described by Barberon et al. (2014) and Gao et al. (2014). FREE1 DEX-RNAi line was generated by Gao et al. (2014). To generate *35S:GFP-PYL4/PYL5 or PYL6* lines, the receptor coding sequence was recombined using the LR reaction into the Gateway-compatible pMDC43 vector (Curtis and Grossniklaus, 2003). To generate *35S:FYVE1-GFP* lines, the *FYVE1* coding sequence was recombined using the LR reaction into the Gateway-compatible pMDC83 vector (Curtis and Grossniklaus, 2003). The pMDC43-PYLs and pMDC83-FYVE1 constructs were transferred to *Agrobacterium tumefaciens* C58C1 (pGV2260) (Deblaere et al., 1985) by electroporation and used to transform Col-0 wild-type plants by the floral dip method (Clough and Bent, 1998). T1 transgenic seeds were selected based on hygromycin resistance and sown in soil to obtain the T2 generation. Homozygous T3 progeny was used for further studies, and expression of GFP-tagged protein was verified by immunoblot analysis using anti-GFP (JL8; Clontech).

Tandem Affinity Purification

Cloning of PYL4 fused to an N-terminal GS^{rhino} tag, which is formed by two IgG binding domains of protein G (G) in front of a streptavidin binding peptide (S) under control of the constitutive cauliflower tobacco mosaic virus 35S promoter, and transformation of Arabidopsis cell suspension cultures were performed as previously described (Van Leene et al., 2015). In GS^{rhino}-PYL4, the G and S modules are separated by two rhinovirus 3C protease cleavage sites, allowing efficient cleavage and elution at 4°C of the S-bait using desthiobiotin. TAP experiments were performed with 25 mg of total protein extract as input as described by Van Leene et al. (2015). Protein interactors were identified by mass spectrometry using an LTQ Orbitrap Velos mass spectrometer (Thermo Fisher Scientific). Proteins with at least two matched high confident peptides were retained. Background proteins were filtered out based on frequency of occurrence of the copurified proteins in a large data set containing 543 TAP experiments using 115 different baits (Van Leene et al., 2015).

Plasmid Constructs

A pENTR223-FYVE1 construct was obtained from the ABRC stock center (clone G12263) and verified by sequencing. It was recombined using the LR reaction into pMDC43 (GFP-FYVE1) and pH7WGR2 (RFP-FYVE1) vectors

(Curtis and Grossniklaus, 2003). Additionally, we amplified the coding sequence of FYVE1 (primers listed in Supplemental Table 1) lacking the stop codon, cloned it into pCR8/GW/TOPO, and verified it by sequencing. This construct was recombined using the LR reaction into pSPYNE-35SGW (FYVE1-myc-YFP^N) and pMDC83 (FYVE1-GFP). The domain architecture of FYVE1 was examined by PCR amplification of the N-terminal (encoding amino acid residues 1 to 395) and C-terminal (396 to 601) FYVE1 regions and cloning into pCR8/GW/TOPO. The pCR8-FYVE1^N or pCR8-FYVE1^C construct was recombined by LR reaction into pGBKT7-GW and pGADT7-GW for Y2H experiments.

The mCherry-ARA7 marker, as well as the corresponding Wave line 2R (Geldner et al., 2009), were obtained from NASC. The RFP-TMD23D-Ub vacuolar marker (Scheuring et al., 2012) was kindly provided by Peter Pimpl (University of Heidelberg). Clones encoding Snf7A, Vps23A, and TOL proteins were obtained from the ABRC. Plasmids used in BY-2 transformation experiments, including mCherry-Vps23A, RFP-Ara7, and Myc-epitope-tagged versions of TOL4 or TOL9, are described elsewhere (Richardson et al., 2011). For BiFC experiments, pCR8-RSL1 was recombined using the LR reaction into pDEST-SCYNE(R) and pCR8-PYR1/PYL4 were recombined into pDEST-SCYCE(R) (Gehl et al., 2009). Additionally, pCR8-RSL1 was recombined into pYFPN43 and pCR8-PYR1/PYL4 was recombined into pYFPC43 (Belda-Palazón et al., 2012; Bueso et al., 2014). The construct expressing CAR1-YFP^N was described previously (Rodriguez et al., 2014).

Transformation of BY-2 Cells

Nicotiana tabacum Bright Yellow-2 (BY-2) suspension cell cultures were maintained and prepared for biolistic bombardment and processed for immunoepifluorescence microscopy analysis as described previously (Lingard et al., 2008; Richardson et al., 2011). Mouse anti-Myc antibodies and goat anti-mouse rhodamine red-X IgGs that were used for immunostaining of BY-2 cells (co)transformed with Myc-TOL4 or -TOL9 were obtained from the Princeton University Monoclonal Antibody Facility and Jackson ImmunoResearch Laboratories, respectively. Imaging of BY-2 cells was performed using an Axioscope 2 MOT epifluorescence microscope (Carl Zeiss) equipped with a Retiga 1300 CCD camera (Qimaging), plus associated Openlab software (Improvision). All fluorescence images of BY-2 cells shown in figures are representative of >25 (co)transformed cells from at least three independent experiments.

Transient Protein Expression Assays in *Nicotiana benthamiana*

Agrobacterium infiltration of tobacco leaves was performed basically as described by Saez et al. (2008). Constructs to investigate the subcellular localization of FYVE1 were produced in pMDC43, pMDC83, and pH7WGR2 (Curtis and Grossniklaus, 2003). To investigate the interaction of FYVE1 and PYR/PYL proteins in planta, we used the pSPYNE-35SGW, pYFP^{N}43, and pYFP^{C}43 vectors (Walter et al., 2004; Belda-Palazón et al., 2012). To investigate the interaction of FYVE1 and Snf7A or Vps23A, we used the pSPYNE-35SGW and pYFP^{C}43 vectors, respectively. The ProCLC2:CLC2-mOrange construct was kindly provided by S.Y. Bednarek (University of Wisconsin). The different binary vectors described in this work were introduced into Agrobacterium C58C1 (pGV2260) or C58C1 (pSOUP) for pGreen-derived vectors by electroporation and transformed cells were selected in Luria Broth (10 g/L Tryptone, 10 g/L NaCl, and 5 g/L yeast extract) plates supplemented with kanamycin (50 μg/mL). They were then grown in liquid Luria Broth to late exponential phase, and cells were harvested by centrifugation and resuspended in 10 mM MES acid-KOH, pH 5.6, containing 10 mM $MgCl_2$ and 150 mM acetosyringone to an OD_{600} of 1. These cells were mixed with an equal volume of Agrobacterium C58C1 (pCH32 35S:p19) expressing the silencing suppressor p19 of tomato bushy stunt virus (Saez et al., 2008) so that the final OD_{600} of the Agrobacterium solution was ~1. Bacteria were incubated for 3 h at room temperature and then injected into young fully expanded leaves of 4-week-old *N. benthamiana* plants. Leaves were examined 48 to 72 h after infiltration using confocal laser scanning microscopy.

Y2H Assays

Protocols were similar to those described previously (Saez et al., 2008). For interaction assays, pairs of bait and prey constructs were cotransformed into yeast strain AH109 according to the manufacturer's instructions (MatchMaker GAL4 Two-Hybrid System; Clontech). Transformed yeast cells were selected on SD/-Leu/-Trp medium, and interactions between two proteins were determined by growing transformed yeast cells on SD/-Leu/-Trp/-His/-Ade medium lacking or supplemented with 50 μM ABA.

CLSM

Confocal imaging was performed using a Zeiss LSM 780 AxioObserver.Z1 laser scanning microscope with a C-Apochromat 40×/1.20 W corrective water immersion objective lens. The following fluorophores were used, and these were excited and fluorescence emission was detected by frame switching in the single or multitracking mode at the indicated wavelengths: SCFP (405 nm/450 to 485 nm), GFP (488 nm/500 to 530 nm), YFP (488 nm/529 to 550 nm), OFP (561 nm/575 to 600 nm), mCherryFP (561 nm/605 to 630 nm), RFP (561 nm/605 to 670), FM4-64 (488 nm/610 to 630 nm), BCECF-AM (488, 510 to 540), and LysoTracker Red (561 nm/585 to 610 nm). For BiFC experiments involving multicolor detection of two fluorescent proteins, sequential imaging of the fluorescent proteins was performed using the sequential channel acquisition mode. Pinholes were adjusted to 1 air unit for each wavelength. Postacquisition image processing was performed using ZEN (ZEISS Efficient Navigation) Lite 2012 imaging software and ImageJ (http://rsb.info.gov/ij/). Fluorescence colocalization analysis was performed using PSC Colocalization plug-in of ImageJ (French et al., 2008). Pearson's and Spearman's correlation in the range +0.4 to 1 indicate colocalization, whereas lower values or negative values indicate lack of colocalization.

For visualization of vacuoles in root epidermal cells, 2-d-old seedlings were incubated in liquid 0.5× Murashige and Skoog (MS) medium (Murashige and Skoog, 1962) containing 5 μM BCECF-AM and 0.02% Pluronic F-127 (Molecular Probes, Invitrogen). After 1 h staining at 22°C in darkness, roots were washed once for 10 min in 0.5× MS medium and BCECF fluorescence was detected using a Zeiss LSM 780 AxioObserver. Z1 laser scanning microscope with C-Apochromat 63×/1.2 W corrective water immersion objective. For 3D reconstruction and surface rendering of BCECF-stained vacuoles, 90 *z*-stack images with 0.2-μm step size were obtained and subsequently processed by using ZEN Lite 2012 imagining software (ZEISS Efficient Navigation) and the ImageJ (http://rsb.info.nih.gov/ij/) plug-in 3D viewer (Schmid et al., 2010; Andrés et al., 2014).

Seed Germination and Seedling Establishment Assays

After surface sterilization of seeds, stratification was conducted in the dark at 4°C for 3 d. Approximately 100 seeds of each genotype were sown on MS plates supplemented with different ABA concentrations depending on the experiment. To score seed germination, radical emergence was analyzed at 72 h after sowing. Seedling establishment was scored as the percentage of seeds that developed green expanded cotyledons and the first pair of true leaves at 5 or 7 d.

Root Growth Assays

Seedlings were grown on vertically oriented MS plates for 4 to 5 d. Afterwards, 20 plants were transferred to new MS plates lacking or supplemented with the indicated concentrations of ABA. The plates were scanned on a flatbed scanner after 10 d to produce image files

suitable for quantitative analysis of root growth using the NIH software ImageJ v1.37.

Water Loss Assays

Water loss assays in 15-d-old seedlings were performed as described (Gonzalez-Guzman et al., 2012). Seedlings were grown in MS plates and five seedlings per genotype with similar growth, three independent experiments, were submitted to the drying atmosphere of a flow laminar hood. Kinetic analysis of water loss was performed and represented as the percentage of initial fresh weight at each scored time point.

Immunopurification of HA-Tagged ABA Receptors and LC-MS/MS-Based Proteomic Analyses

Proteins from plants expressing HA-tagged versions of PYR1/PYL4/PYL8 receptors were immunopurified by incubation with μMACS magnetic beads coated with anti-HA antibodies (Miltenyi Biotec) in at least three independent experiments for each HA-tagged receptor (Bueso et al., 2014; Castillo et al., 2015). As a negative control, we performed IP of protein extracts prepared from plants transformed with an empty pAlligator2 vector, which express only the triple HA epitope. In a first round of experiments, immunopurified and coimmunopurified proteins were precipitated using cold acetone and digested overnight with trypsin (mass spectrometry grade; Promega; 1/10 enzyme/substrate ratio), and the resulting peptides were desalted with UltraMicroSpin columns and fragmented by collision-induced dissociation in a Thermo LTQ Orbitrap Velos Pro mass spectrometer. Fragmented peptides were separated in a packed nano-capillary column (NTCC-360/75-1.9-25L Nikkyo Technos). Raw data were processed and analyzed by using the Mascot Server v2.4.3 (Matrix Science) database with Sequest search engine. Identified peptides were filtered by XCorr (z=2 XCorr>0.9, z=3 XCorr>1.2, z>4 XCorr>1.5) and deltaCN > 0.15. The maximum number of missed cleavages was three, and the MS and MS/MS tolerances were 0.5 and 0.7, respectively. In a second round of experiments, immunoprecipitated samples were eluted in Laemmli buffer, run on a 1D 10% polyacrylamide gel (Any-KD; Bio-Rad), and stained with colloidal Coomassie Brilliant Blue dye. The gel slices were cut and digested in the gel with trypsin (mass spectrometry grade) as described (Shevchenko et al., 1996). The digestion was stopped with 1% trifluoroacetic acid (TFA) and was followed by a double extraction with acetonitrile (ACN). Next, all the peptide solutions were combined and dried in a rotary evaporator. Samples were resuspended in an adequate volume of 2% ACN containing 0.1% TFA, and 5 μL of each sample was loaded onto a trap column (NanoLC column, 3 μ C18-CL, 350 μm × 0.5 mm; Eksigen) and desalted with 0.1% TFA at 3 μL/min for 5 min. The peptides were then loaded onto an analytical column (LC column, 3 μ C18-CL, 75 μm × 12 cm; Nikkyo) equilibrated in 5% ACN 0.1% formic acid. Elution was performed with a linear gradient of 5 to 35% ACN in 0.1% formic acid for 120 min at a flow rate of 300 nL/min. Peptides were analyzed in a nanoESI qQTOF mass spectrometer (6600 Triple TOF; AB Sciex). The triple TOF was operated in information-dependent acquisition mode, in which a 0.26-s TOF MS scan from 350 to 1250 *m/z* was performed, followed by 0.05-s product ion scans from 100 to 1600 *m/z* on the 50 most intense 2-5 charged ions. ProteinPilot default parameters were used to generate a peak list directly from 6600 TripleTof wiff files. The Paragon algorithm of ProteinPilot Software version 5.0, a database search engine for the identification of peptides from tandem mass spectrometry data (Shilov et al., 2007), was used to search the Expasy protein database using the following parameters: trypsin specificity, Cys-alkylation (IAM), no taxonomy restriction, and the search effort set to through. To avoid the use of the same spectral evidence in more than one protein, the identified proteins are grouped based on MS/MS spectra by the ProteinPilot Progroup algorithm. The protein of each group that can explain more spectral data with confidence is shown as the primary protein of the group. Proteins showing Unused ProtScore >2.0 were identified with confidence ≥99% according to the following equation: ProtScore = −log[1 − (percentage of confidence/100)].

Drug Treatment and Staining with Fluorescent Probes

Drugs or fluorescent probes were applied to 4-d-old seedlings in liquid MS medium supplemented with BFA (Sigma-Aldrich; 50 μM), WM (Sigma-Aldrich; 33 μM), TyrA23 (Sigma-Aldrich; 33 μM), ConA (Sigma-Aldrich; 0.5 μM), the acidotropic dye LysoTracker Red DND-99 (Molecular Probes; 2 μM), or the endocytic tracer FM4-64 (Biotium; 4 μM). All chemicals were dissolved in DMSO and controls contained an equivalent amount of solvent. Experiments were performed at least in triplicate, with a minimum of eight individuals.

For detection of GFP-PYL4/PYL5/PYL6 accumulation in BFA bodies, the seedlings were firstly pulse labeled with 4 μM FM4-64 for 10 min, followed by incubation with BFA for 1 h. WM and LysoTracker Red DND-99 were applied simultaneously and visualized after 50 min. ConA was applied 50 min before addition of LysoTracker Red DND-99 for additional 50 min. To analyze vacuolar morphology, seedlings were first incubated for 3 h in MS medium with 4 μM FM4-64 and then washed twice with fresh medium before confocal imagining.

Protein Extraction, Analysis, Immunodetection, and Affinity Purification of Ubiquitylated Proteins

Protein extracts for immunodetection experiments were prepared from Arabidopsis transgenic lines expressing GFP- or HA-tagged PYL4 in the indicated genetic backgrounds. Material (~100 mg) for direct immunoblot analysis was extracted in 2× Laemmli buffer (125 mM Tris-HCl, pH 6.8, 4% SDS, 20% glycerol, 2% mercaptoethanol, and 0.001% bromophenol blue), and proteins were run in a 4 to 15% SDS-PAGE MiniProtean precast gel (Bio-Rad) and analyzed by immunoblotting. Proteins were transferred onto Immobilon-P membranes (Millipore) and probed with an anti-HA-peroxidase (Roche) or an anti-GFP monoclonal antibody (clone JL-8; Clontech) as primary antibody and ECL anti-mouse peroxidase (GE Healthcare) as secondary antibody. Antibodies were used at a 1:10,000 dilution except for the anti-CHC1,2 antibody (Agrisera 10690), which was used at 1:1000. In this case, after incubation for 2 h at 4°C, immunoprecipitation of CHC was achieved by adding 50 μL of Dynabeads Protein G (Life Technologies) and overnight incubation. Detection was performed using the ECL Advanced Western Blotting Chemiluminiscent Detection kit (GE Healthcare). Image capture was done using the image analyzer LAS3000, and quantification of the protein signal was done using Image Guache V4.0 software.

For immunoblot analysis of GFP-PYL4 vacuolar delivery, 35S::GFP-PYL4 seedlings grown in liquid MS medium for 15 d were mock treated or treated with 20 or 100 μM E64 (Sigma-Aldrich; dissolved in water) for 4 h. Plant material was collected and frozen in liquid nitrogen. Protein extracts were prepared using a modified PBS buffer (140 mM NaCl, 10 mM KCl, 8 mM Na_2HPO_4, 2 mM NaH_2PO_4, 1 mM EDTA, 0.1% Triton X-100, and protease inhibitor cocktail), followed by centrifugation at 12,000*g* for 20 min at 4°C. The supernatant was used for SDS-PAGE and immunoblot analysis.

Affinity purification of ubiquitylated proteins using p62-agarose was performed as described by Bueso et al. (2014). Immunodetection of ubiquitylated proteins was performed using an anti-Ub antibody (Ub P4D1: sc-8017; Santa Cruz Biotechnology). The DEX-inducible FREE1-RNAi plants expressing GFP-PYL4 were germinated on 0.5× MS plates with or without 10 μM DEX. The 7-d-old plants were ground in liquid nitrogen, and total proteins were extracted in IP buffer (50 mM Tris-HCl, pH 7.4, 150 mM NaCl, 0.5 mM EDTA, 0.2% Nonidet P-40, 5% glycerol, and 1× Complete Protease Inhibitor Cocktail [Roche]). The cell lysates were then incubated with GFP-Trap magnetic beads (ChromoTek) for 4 h at 4°C in a top to end rotator. After incubation, the beads were washed four times with ice-cold washing buffer (10 mM Tris-HCl, pH 7.4, 150 mM NaCl, 0.5 mM EDTA, and 0.05% Nonidet P-40) and then eluted by boiling in reducing SDS sample

buffer. Samples were separated by SDS-PAGE and analyzed by immunoblot using appropriate antibodies.

Accession Numbers

The Arabidopsis Genome Initiative locus identifiers are as follows: FYVE1/FREE1, At1g20110; Snf7A, At2g19830; Vps23A, At3g12400; TOL4, At1g76970; TOL9, At4g32760; PYR1, At4g17870; and PYL4, At2g38310. Proteomics data were deposited to the ProteomeXchange Consortium through the PRIDE partner repository with the data set identifiers PXD002396 and 10.6019/PXD002396. T-DNA insertion lines *fyve1-3* (SAIL_516_E05) and *fyve1-4* (SALK_205349) were obtained from the Nottingham Arabidopsis Stock Centre (http://nasc.nott.ac.uk). *fyve1-1/free1* (pst18264/15-1960 RIKEN BRC) was described by Barberon et al. (2014) and Gao et al. (2014). The FREE1 DEX-RNAi line was generated by Gao et al. (2014).

Supplemental Data

Supplemental Figure 1. Identification and Modeling of the FYVE Domain in At1g20110/FYVE1/FREE1.

Supplemental Figure 2. Analysis of FYVE1 Using PSIPRED and DISOPRED2 Prediction Servers Reveals the Presence of an IDR in the N-Terminal Region of the Protein.

Supplemental Figure 3. Interaction of PYR1 and CAR1 Generates Punctate/Globular Structures Near the Plasma Membrane That Colocalize with RFP-FYVE1.

Supplemental Figure 4. In Planta Interaction of FYVE1 and Vps23A and Colocalization of FYVE1 and ARA7 in BY-2 Cells.

Supplemental Figure 5. GFP-PYL5 Accumulates in BFA Bodies and Both GFP-PYL4 and GFP-PYL5 Can Be Found in Lytic Compartments.

Supplemental Figure 6. GFP-PYL6 Accumulates in BFA Bodies and Lytic Compartments.

Supplemental Figure 7. Diagram *FYVE1* and Location of the Primers Used for qRT-PCR Analysis of *FYVE1* Expression.

Supplemental Figure 8. Altered Vacuolar Morphology in *fyve1* Alleles.

Supplemental Figure 9. Analysis of *HA-PYL4* and *GFP-PYL4* mRNA Expression and CLSM Imaging of GFP-PYL4.

Supplemental Table 1. List of Oligonucleotides Used in This Work.

Supplemental Data Set 1. Results Obtained in TAP Experiments and Peptide Identification Using the LTQ Orbitrap Velos and Mascot Distiller Software.

Supplemental Movie 1. Movie Depicting CLSM Imaging of GFP-PYL4 Expressed in *N. benthamiana*.

Supplemental Movie 2. Movie Depicting CLSM Imaging of FYVE1-GFP and RFP-PYL4 Expressed in *N. benthamiana*.

ACKNOWLEDGMENTS

Work in P.L.R.'s laboratory was supported by the Ministerio de Ciencia e Innovacion, Fondo Europeo de Desarrollo Regional and Consejo Superior de Investigaciones Cientificas (Grant BIO2014-52537-R). Work in R.T.M.'s laboratory was supported by a grant from the Natural Sciences and Engineering Research Council of Canada and a University of Guelph Research Chair. Work in J.L.'s laboratory was supported by the Ministerio de Ciencia e Innovacion and Fondo Europeo de Desarrollo Regional Grants BIO2011-27526 and BIO2014-56067-P. L.R. was supported by a FPI fellowship and M.G.-G. by a JAE-DOC research contract. Work in L.J.'s laboratory was supported by grants from the Research Grants Council of Hong Kong (C4011-14R and AoE/M-05/12). We thank S.Y. Bednarek for the ProCLC2:CLC2-mOrange construct.

AUTHOR CONTRIBUTIONS

P.L.R. conceived the project. B.B.-P., L.R., M.A.F., M.-C.C., E.M.A., C.G., M.G.-G., M.P.-L., Q.Z., N.D.W., and K.G. performed research. B.B.-P., L.R., M.A.F., M.-C.C., E.M.A., C.G., M.G.-G., Q.Z., N.D.W., K.G., G.D.J., L.J., J.L., R.T.M., and P.L.R. analyzed data. P.L.R. wrote the article with input from G.D.J., C.G., L.J., J.L., and R.T.M.

Received March 7, 2016; revised July 6, 2016; accepted August 4, 2016; published August 5, 2016.

REFERENCES

Abas, L., Benjamins, R., Malenica, N., Paciorek, T., Wiśniewska, J., Moulinier-Anzola, J.C., Sieberer, T., Friml, J., and Luschnig, C. (2006). Intracellular trafficking and proteolysis of the *Arabidopsis* auxin-efflux facilitator PIN2 are involved in root gravitropism. Nat. Cell Biol. **8:** 249–256.

Andrés, Z., Pérez-Hormaeche, J., Leidi, E.O., Schlücking, K., Steinhorst, L., McLachlan, D.H., Schumacher, K., Hetherington, A.M., Kudla, J., Cubero, B., and Pardo, J.M. (2014). Control of vacuolar dynamics and regulation of stomatal aperture by tonoplast potassium uptake. Proc. Natl. Acad. Sci. USA **111:** E1806–E1814.

Antoni, R., Gonzalez-Guzman, M., Rodriguez, L., Peirats-Llobet, M., Pizzio, G.A., Fernandez, M.A., De Winne, N., De Jaeger, G., Dietrich, D., Bennett, M.J., and Rodriguez, P.L. (2013). PYRABACTIN RESISTANCE1-LIKE8 plays an important role for the regulation of abscisic acid signaling in root. Plant Physiol. **161:** 931–941.

Barberon, M., Zelazny, E., Robert, S., Conéjéro, G., Curie, C., Friml, J., and Vert, G. (2011). Monoubiquitin-dependent endocytosis of the iron-regulated transporter 1 (IRT1) transporter controls iron uptake in plants. Proc. Natl. Acad. Sci. USA **108:** E450–E458.

Barberon, M., Dubeaux, G., Kolb, C., Isono, E., Zelazny, E., and Vert, G. (2014). Polarization of IRON-REGULATED TRANSPORTER 1 (IRT1) to the plant-soil interface plays crucial role in metal homeostasis. Proc. Natl. Acad. Sci. USA **111:** 8293–8298.

Belda-Palazón, B., Ruiz, L., Martí, E., Tárraga, S., Tiburcio, A.F., Culiáñez, F., Farràs, R., Carrasco, P., and Ferrando, A. (2012). Aminopropyltransferases involved in polyamine biosynthesis localize preferentially in the nucleus of plant cells. PLoS One **7:** e46907.

Brandt, B., Munemasa, S., Wang, C., Nguyen, D., Yong, T., Yang, P.G., Poretsky, E., Belknap, T.F., Waadt, R., Aleman, F., and Schroeder, J.I. (2015). Calcium specificity signaling mechanisms in abscisic acid signal transduction in Arabidopsis guard cells. eLife **4:** e03599.

Bueso, E., Rodriguez, L., Lorenzo-Orts, L., Gonzalez-Guzman, M., Sayas, E., Muñoz-Bertomeu, J., Ibañez, C., Serrano, R., and Rodriguez, P.L. (2014). The single-subunit RING-type E3 ubiquitin ligase RSL1 targets PYL4 and PYR1 ABA receptors in plasma membrane to modulate abscisic acid signaling. Plant J. **80:** 1057–1071.

Cardona-López, X., Cuyas, L., Marín, E., Rajulu, C., Irigoyen, M.L., Gil, E., Puga, M.I., Bligny, R., Nussaume, L., Geldner, N., Paz-Ares,

J., and Rubio, V. (2015). ESCRT-III-associated protein ALIX mediates high-affinity phosphate transporter trafficking to maintain phosphate homeostasis in *Arabidopsis.* Plant Cell **27:** 2560–2581.

Cashikar, A.G., Shim, S., Roth, R., Maldazys, M.R., Heuser, J.E., and Hanson, P.I. (2014). Structure of cellular ESCRT-III spirals and their relationship to HIV budding. eLife **3:** 3.

Castillo, M.C., Lozano-Juste, J., González-Guzmán, M., Rodriguez, L., Rodriguez, P.L., and León, J. (2015). Inactivation of PYR/PYL/RCAR ABA receptors by tyrosine nitration may enable rapid inhibition of ABA signaling by nitric oxide in plants. Sci. Signal. **8:** ra89.

Chen, X., Irani, N.G., and Friml, J. (2011). Clathrin-mediated endocytosis: the gateway into plant cells. Curr. Opin. Plant Biol. **14:** 674–682.

Clough, S.J., and Bent, A.F. (1998). Floral dip: a simplified method for Agrobacterium-mediated transformation of *Arabidopsis thaliana*. Plant J. **16:** 735–743.

Curtis, M.D., and Grossniklaus, U. (2003). A gateway cloning vector set for high-throughput functional analysis of genes in planta. Plant Physiol. **133:** 462–469.

Cutler, S.R., Rodriguez, P.L., Finkelstein, R.R., and Abrams, S.R. (2010). Abscisic acid: emergence of a core signaling network. Annu. Rev. Plant Biol. **61:** 651–679.

daSilva, L.L., Taylor, J.P., Hadlington, J.L., Hanton, S.L., Snowden, C.J., Fox, S.J., Foresti, O., Brandizzi, F., and Denecke, J. (2005). Receptor salvage from the prevacuolar compartment is essential for efficient vacuolar protein targeting. Plant Cell **17:** 132–148.

Deblaere, R., Bytebier, B., De Greve, H., Deboeck, F., Schell, J., Van Montagu, M., and Leemans, J. (1985). Efficient octopine Ti plasmid-derived vectors for *Agrobacterium*-mediated gene transfer to plants. Nucleic Acids Res. **13:** 4777–4788.

Demir, F., Horntrich, C., Blachutzik, J.O., Scherzer, S., Reinders, Y., Kierszniowska, S., Schulze, W.X., Harms, G.S., Hedrich, R., Geiger, D., and Kreuzer, I. (2013). *Arabidopsis* nanodomain-delimited ABA signaling pathway regulates the anion channel SLAH3. Proc. Natl. Acad. Sci. USA **110:** 8296–8301.

Diaz, M., et al. (2016). Calcium-dependent oligomerization of CAR proteins at cell membrane modulates ABA signaling. Proc. Natl. Acad. Sci. USA **113:** E396–E405.

Di Rubbo, S., et al. (2013). The clathrin adaptor complex AP-2 mediates endocytosis of brassinosteroid insensitive1 in *Arabidopsis.* Plant Cell **25:** 2986–2997.

Dhonukshe, P., Aniento, F., Hwang, I., Robinson, D.G., Mravec, J., Stierhof, Y.D., and Friml, J. (2007). Clathrin-mediated constitutive endocytosis of PIN auxin efflux carriers in Arabidopsis. Curr. Biol. **17:** 520–527.

Finkelstein, R. (2013). Abscisic acid synthesis and response. Arabidopsis Book **11:** e0166.

French, A.P., Mills, S., Swarup, R., Bennett, M.J., and Pridmore, T.P. (2008). Colocalization of fluorescent markers in confocal microscope images of plant cells. Nat. Protoc. **3:** 619–628.

Gadeyne, A., et al. (2014). The TPLATE adaptor complex drives clathrin-mediated endocytosis in plants. Cell **156:** 691–704.

Gao, C., Luo, M., Zhao, Q., Yang, R., Cui, Y., Zeng, Y., Xia, J., and Jiang, L. (2014). A unique plant ESCRT component, FREE1, regulates multivesicular body protein sorting and plant growth. Curr. Biol. **24:** 2556–2563.

Gao, C., Zhuang, X., Cui, Y., Fu, X., He, Y., Zhao, Q., Zeng, Y., Shen, J., Luo, M., and Jiang, L. (2015). Dual roles of an *Arabidopsis* ESCRT component FREE1 in regulating vacuolar protein transport and autophagic degradation. Proc. Natl. Acad. Sci. USA **112:** 1886–1891.

Gaullier, J.M., Simonsen, A., D'Arrigo, A., Bremnes, B., Stenmark, H., and Aasland, R. (1998). FYVE fingers bind PtdIns(3)P. Nature **394:** 432–433.

Gehl, C., Waadt, R., Kudla, J., Mendel, R.R., and Hänsch, R. (2009). New GATEWAY vectors for high throughput analyses of protein-protein interactions by bimolecular fluorescence complementation. Mol. Plant **2:** 1051–1058.

Geiger, D., Scherzer, S., Mumm, P., Stange, A., Marten, I., Bauer, H., Ache, P., Matschi, S., Liese, A., Al-Rasheid, K.A., Romeis, T., and Hedrich, R. (2009). Activity of guard cell anion channel SLAC1 is controlled by drought-stress signaling kinase-phosphatase pair. Proc. Natl. Acad. Sci. USA **106:** 21425–21430.

Geldner, N., Dénervaud-Tendon, V., Hyman, D.L., Mayer, U., Stierhof, Y.D., and Chory, J. (2009). Rapid, combinatorial analysis of membrane compartments in intact plants with a multicolor marker set. Plant J. **59:** 169–178.

Göhre, V., Spallek, T., Häweker, H., Mersmann, S., Mentzel, T., Boller, T., de Torres, M., Mansfield, J.W., and Robatzek, S. (2008). Plant pattern-recognition receptor FLS2 is directed for degradation by the bacterial ubiquitin ligase AvrPtoB. Curr. Biol. **18:** 1824–1832.

Gonzalez-Guzman, M., Pizzio, G.A., Antoni, R., Vera-Sirera, F., Merilo, E., Bassel, G.W., Fernandez, M.A., Holdsworth, M.J., Perez-Amador, M.A., Kollist, H., and Rodriguez, P.L. (2012). Arabidopsis PYR/PYL/RCAR receptors play a major role in quantitative regulation of stomatal aperture and transcriptional response to abscisic acid. Plant Cell **24:** 2483–2496.

Grondin, A., Rodrigues, O., Verdoucq, L., Merlot, S., Leonhardt, N., and Maurel, C. (2015). Aquaporins contribute to ABA-triggered stomatal closure through OST1-mediated phosphorylation. Plant Cell **27:** 1945–1954.

Hanson, P.I., and Cashikar, A. (2012). Multivesicular body morphogenesis. Annu. Rev. Cell Dev. Biol. **28:** 337–362.

Imes, D., Mumm, P., Böhm, J., Al-Rasheid, K.A., Marten, I., Geiger, D., and Hedrich, R. (2013). Open stomata 1 (OST1) kinase controls R-type anion channel QUAC1 in *Arabidopsis* guard cells. Plant J. **74:** 372–382.

Irigoyen, M.L., et al. (2014). Targeted degradation of abscisic acid receptors is mediated by the ubiquitin ligase substrate adaptor DDA1 in *Arabidopsis.* Plant Cell **26:** 712–728.

Jelínková, A., Malínská, K., Simon, S., Kleine-Vehn, J., Parezová, M., Pejchar, P., Kubes, M., Martinec, J., Friml, J., Zazímalová, E., and Petrásek, J. (2010). Probing plant membranes with FM dyes: tracking, dragging or blocking? Plant J. **61:** 883–892.

Jones, A.M., et al. (2014). Border control–a membrane-linked interactome of *Arabidopsis.* Science **344:** 711–716.

Kasai, K., Takano, J., Miwa, K., Toyoda, A., and Fujiwara, T. (2011). High boron-induced ubiquitination regulates vacuolar sorting of the BOR1 borate transporter in *Arabidopsis thaliana*. J. Biol. Chem. **286:** 6175–6183.

Kolb, C., Nagel, M.K., Kalinowska, K., Hagmann, J., Ichikawa, M., Anzenberger, F., Alkofer, A., Sato, M.H., Braun, P., and Isono, E. (2015). FYVE1 is essential for vacuole biogenesis and intracellular trafficking in *Arabidopsis.* Plant Physiol. **167:** 1361–1373.

Konopka, C.A., Backues, S.K., and Bednarek, S.Y. (2008). Dynamics of Arabidopsis dynamin-related protein 1C and a clathrin light chain at the plasma membrane. Plant Cell **20:** 1363–1380.

Korbei, B., Moulinier-Anzola, J., De-Araujo, L., Lucyshyn, D., Retzer, K., Khan, M.A., and Luschnig, C. (2013). *Arabidopsis* TOL proteins act as gatekeepers for vacuolar sorting of PIN2 plasma membrane protein. Curr. Biol. **23:** 2500–2505.

Kwak, J.M., Mori, I.C., Pei, Z.M., Leonhardt, N., Torres, M.A., Dangl, J.L., Bloom, R.E., Bodde, S., Jones, J.D., and Schroeder, J.I. (2003). NADPH oxidase AtrbohD and AtrbohF genes function in ROS-dependent ABA signaling in *Arabidopsis.* EMBO J. **22:** 2623–2633.

Lee, H.K., Cho, S.K., Son, O., Xu, Z., Hwang, I., and Kim, W.T. (2009a). Drought stress-induced Rma1H1, a RING membrane-anchor E3

ubiquitin ligase homolog, regulates aquaporin levels via ubiquitination in transgenic *Arabidopsis* plants. Plant Cell **21:** 622–641.

Lee, S.C., Lan, W., Buchanan, B.B., and Luan, S. (2009b). A protein kinase-phosphatase pair interacts with an ion channel to regulate ABA signaling in plant guard cells. Proc. Natl. Acad. Sci. USA **106:** 21419–21424.

Leitner, J., Petrášek, J., Tomanov, K., Retzer, K., Pařezová, M., Korbei, B., Bachmair, A., Zažímalová, E., and Luschnig, C. (2012). Lysine63-linked ubiquitylation of PIN2 auxin carrier protein governs hormonally controlled adaptation of *Arabidopsis* root growth. Proc. Natl. Acad. Sci. USA **109:** 8322–8327.

Lemmon, M.A. (2008). Membrane recognition by phospholipid-binding domains. Nat. Rev. Mol. Cell Biol. **9:** 99–111.

Lingard, M.J., Gidda, S.K., Bingham, S., Rothstein, S.J., Mullen, R.T., and Trelease, R.N. (2008). *Arabidopsis* PEROXIN11c-e, FISSION1b, and DYNAMIN-RELATED PROTEIN3A cooperate in cell cycle-associated replication of peroxisomes. Plant Cell **20:** 1567–1585.

Ma, Y., Szostkiewicz, I., Korte, A., Moes, D., Yang, Y., Christmann, A., and Grill, E. (2009). Regulators of PP2C phosphatase activity function as abscisic acid sensors. Science **324:** 1064–1068.

MacGurn, J.A., Hsu, P.C., and Emr, S.D. (2012). Ubiquitin and membrane protein turnover: from cradle to grave. Annu. Rev. Biochem. **81:** 231–259.

Martin-Serrano, J., Yarovoy, A., Perez-Caballero, D., and Bieniasz, P.D. (2003). Divergent retroviral late-budding domains recruit vacuolar protein sorting factors by using alternative adaptor proteins. Proc. Natl. Acad. Sci. USA **100:** 12414–12419.

Martins, S., Dohmann, E.M., Cayrel, A., Johnson, A., Fischer, W., Pojer, F., Satiat-Jeunemaître, B., Jaillais, Y., Chory, J., Geldner, N., and Vert, G. (2015). Internalization and vacuolar targeting of the brassinosteroid hormone receptor BRI1 are regulated by ubiquitination. Nat. Commun. **6:** 6151.

Merlot, S., Leonhardt, N., Fenzi, F., Valon, C., Costa, M., Piette, L., Vavasseur, A., Genty, B., Boivin, K., Müller, A., Giraudat, J., and Leung, J. (2007). Constitutive activation of a plasma membrane H(+)-ATPase prevents abscisic acid-mediated stomatal closure. EMBO J. **26:** 3216–3226.

Misra, S., and Hurley, J.H. (1999). Crystal structure of a phosphatidylinositol 3-phosphate-specific membrane-targeting motif, the FYVE domain of Vps27p. Cell **97:** 657–666.

Murashige, T., and Skoog, F. (1962). A revised medium for rapid growth and bioassays with tobacco tissue culture. Physiol. Plant. **15:** 473–497.

Murphy, A.S., Bandyopadhyay, A., Holstein, S.E., and Peer, W.A. (2005). Endocytotic cycling of PM proteins. Annu. Rev. Plant Biol. **56:** 221–251.

Nodzynski, T., Feraru, M.I., Hirsch, S., De Rycke, R., Niculaes, C., Boerjan, W., Van Leene, J., De Jaeger, G., Vanneste, S., and Friml, J. (2013). Retromer subunits VPS35A and VPS29 mediate prevacuolar compartment (PVC) function in *Arabidopsis.* Mol. Plant **6:** 1849–1862.

Odorizzi, G. (2006). The multiple personalities of Alix. J. Cell Sci. **119:** 3025–3032.

Pali, T., Whyteside, G., Dixon, N., Kee, T.P., Ball, S., Harrison, M.A., Findlay, J.B., Finbow, M.E., and Marsh, D. (2004). Interaction of inhibitors of the vacuolar H(+)-ATPase with the transmembrane Vo-sector. Biochemistry **43:** 12297–12305.

Park, S.Y., et al. (2009). Abscisic acid inhibits type 2C protein phosphatases via the PYR/PYL family of START proteins. Science **324:** 1068–1071.

Paez Valencia, J., Goodman, K., and Otegui, M.S. (2016). Endocytosis and endosomal trafficking in plants. Annu. Rev. Plant Biol. **67:** 309–335.

Peel, S., Macheboeuf, P., Martinelli, N., and Weissenhorn, W. (2011). Divergent pathways lead to ESCRT-III-catalyzed membrane fission. Trends Biochem. Sci. **36:** 199–210.

Peirats-Llobet, M., Han, S.K., Gonzalez-Guzman, M., Jeong, C.W., Rodriguez, L., Belda-Palazon, B., Wagner, D., and Rodriguez, P.L. (2016). A direct link between abscisic acid sensing and the chromatin remodeling ATPase BRAHMA via core ABA signaling pathway components. Mol. Plant **9:** 136–147.

Pizzio, G.A., Rodriguez, L., Antoni, R., Gonzalez-Guzman, M., Yunta, C., Merilo, E., Kollist, H., Albert, A., and Rodriguez, P.L. (2013). The PYL4 A194T mutant uncovers a key role of PYR1-LIKE4/PROTEIN PHOSPHATASE 2CA interaction for abscisic acid signaling and plant drought resistance. Plant Physiol. **163:** 441–455.

Planes, M.D., Niñoles, R., Rubio, L., Bissoli, G., Bueso, E., García-Sánchez, M.J., Alejandro, S., Gonzalez-Guzmán, M., Hedrich, R., Rodriguez, P.L., Fernández, J.A., and Serrano, R. (2015). A mechanism of growth inhibition by abscisic acid in germinating seeds of *Arabidopsis* thaliana based on inhibition of plasma membrane H^+-ATPase and decreased cytosolic pH, K^+, and anions. J. Exp. Bot. **66:** 813–825.

Pornillos, O., Alam, S.L., Rich, R.L., Myszka, D.G., Davis, D.R., and Sundquist, W.I. (2002). Structure and functional interactions of the Tsg101 UEV domain. EMBO J. **21:** 2397–2406.

Raiborg, C., Bache, K.G., Mehlum, A., Stang, E., and Stenmark, H. (2001). Hrs recruits clathrin to early endosomes. EMBO J. **20:** 5008–5021.

Raiborg, C., Bache, K.G., Gillooly, D.J., Madshus, I.H., Stang, E., and Stenmark, H. (2002). Hrs sorts ubiquitinated proteins into clathrin-coated microdomains of early endosomes. Nat. Cell Biol. **4:** 394–398.

Raiborg, C., and Stenmark, H. (2009). The ESCRT machinery in endosomal sorting of ubiquitylated membrane proteins. Nature **458:** 445–452.

Richardson, L.G., Howard, A.S., Khuu, N., Gidda, S.K., McCartney, A., Morphy, B.J., and Mullen, R.T. (2011). Protein-protein interaction network and subcellular localization of the *Arabidopsis thaliana* ESCRT machinery. Front. Plant Sci. **2:** 20.

Richardson, L.G., Clendening, E.A., Sheen, H., Gidda, S.K., White, K.A., and Mullen, R.T. (2014). A unique N-terminal sequence in the Carnation Italian ringspot virus p36 replicase-associated protein interacts with the host cell ESCRT-I component Vps23. J. Virol. **88:** 6329–6344.

Robinson, D.G., Jiang, L., and Schumacher, K. (2008). The endosomal system of plants: charting new and familiar territories. Plant Physiol. **147:** 1482–1492.

Rodriguez, L., Gonzalez-Guzman, M., Diaz, M., Rodrigues, A., Izquierdo-Garcia, A.C., Peirats-Llobet, M., Fernandez, M.A., Antoni, R., Fernandez, D., Marquez, J.A., Mulet, J. M., Albert, A., and Rodriguez, P.L. (2014). C2-domain abscisic acid-related proteins mediate the interaction of PYR/PYL/RCAR abscisic acid receptors with the plasma membrane and regulate abscisic acid sensitivity in *Arabidopsis*. Plant Cell **26:** 4802–4820.

Saez, A., Robert, N., Maktabi, M.H., Schroeder, J.I., Serrano, R., and Rodriguez, P.L. (2006). Enhancement of abscisic acid sensitivity and reduction of water consumption in Arabidopsis by combined inactivation of the protein phosphatases type 2C ABI1 and HAB1. Plant Physiol. **141:** 1389–1399.

Saez, A., Rodrigues, A., Santiago, J., Rubio, S., and Rodriguez, P.L. (2008). HAB1-SWI3B interaction reveals a link between abscisic acid signaling and putative SWI/SNF chromatin-remodeling complexes in *Arabidopsis.* Plant Cell **20:** 2972–2988.

Santiago, J., Rodrigues, A., Saez, A., Rubio, S., Antoni, R., Dupeux, F., Park, S.Y., Márquez, J.A., Cutler, S.R., and Rodriguez, P.L. (2009). Modulation of drought resistance by the abscisic acid

receptor PYL5 through inhibition of clade A PP2Cs. Plant J. **60:** 575–588.

Sato, A., Sato, Y., Fukao, Y., Fujiwara, M., Umezawa, T., Shinozaki, K., Hibi, T., Taniguchi, M., Miyake, H., Goto, D.B., and Uozumi, N. (2009). Threonine at position 306 of the KAT1 potassium channel is essential for channel activity and is a target site for ABA-activated SnRK2/OST1/SnRK2.6 protein kinase. Biochem. J. **424:** 439–448.

Scheuring, D., Künzl, F., Viotti, C., Yan, M.S., Jiang, L., Schellmann, S., Robinson, D.G., and Pimpl, P. (2012). Ubiquitin initiates sorting of Golgi and plasma membrane proteins into the vacuolar degradation pathway. BMC Plant Biol. **12:** 164.

Schmid, B., Schindelin, J., Cardona, A., Longair, M., and Heisenberg, M. (2010). A high-level 3D visualization API for Java and ImageJ. BMC Bioinformatics **11:** 274.

Shevchenko, A., Jensen, O.N., Podtelejnikov, A.V., Sagliocco, F., Wilm, M., Vorm, O., Mortensen, P., Shevchenko, A., Boucherie, H., and Mann, M. (1996). Linking genome and proteome by mass spectrometry: large-scale identification of yeast proteins from two dimensional gels. Proc. Natl. Acad. Sci. USA **93:** 14440–14445.

Shilov, I.V., Seymour, S.L., Patel, A.A., Loboda, A., Tang, W.H., Keating, S.P., Hunter, C.L., Nuwaysir, L.M., and Schaeffer, D.A. (2007). The Paragon Algorithm, a next generation search engine that uses sequence temperature values and feature probabilities to identify peptides from tandem mass spectra. Mol. Cell. Proteomics **6:** 1638–1655.

Sirichandra, C., Gu, D., Hu, H.C., Davanture, M., Lee, S., Djaoui, M., Valot, B., Zivy, M., Leung, J., Merlot, S., and Kwak, J.M. (2009). Phosphorylation of the *Arabidopsis* AtrbohF NADPH oxidase by OST1 protein kinase. FEBS Lett. **583:** 2982–2986.

Spitzer, C., Reyes, F.C., Buono, R., Sliwinski, M.K., Haas, T.J., and Otegui, M.S. (2009). The ESCRT-related CHMP1A and B proteins mediate multivesicular body sorting of auxin carriers in *Arabidopsis* and are required for plant development. Plant Cell **21:** 749–766.

Stenmark, H., Aasland, R., and Driscoll, P.C. (2002). The phosphatidylinositol 3-phosphate-binding FYVE finger. FEBS Lett. **513:** 77–84.

Strack, B., Calistri, A., Craig, S., Popova, E., and Göttlinger, H.G. (2003). AIP1/ALIX is a binding partner for HIV-1 p6 and EIAV p9 functioning in virus budding. Cell **114:** 689–699.

Sutter, J.U., Sieben, C., Hartel, A., Eisenach, C., Thiel, G., and Blatt, M.R. (2007). Abscisic acid triggers the endocytosis of the *arabidopsis* KAT1 K^+ channel and its recycling to the plasma membrane. Curr. Biol. **17:** 1396–1402.

Tamura, K., Shimada, T., Ono, E., Tanaka, Y., Nagatani, A., Higashi, S.I., Watanabe, M., Nishimura, M., and Hara-Nishimura, I. (2003). Why green fluorescent fusion proteins have not been observed in the vacuoles of higher plants. Plant J. **35:** 545–555.

Teis, D., Saksena, S., and Emr, S.D. (2009). SnapShot: the ESCRT machinery. Cell **137:** 182–182.e1.

Umezawa, T., Sugiyama, N., Takahashi, F., Anderson, J.C., Ishihama, Y., Peck, S.C., and Shinozaki, K. (2013). Genetics and phosphoproteomics reveal a protein phosphorylation network in the abscisic acid signaling pathway in *Arabidopsis thaliana*. Sci. Signal. **6:** rs8.

Van Leene, J., et al. (2015). An improved toolbox to unravel the plant cellular machinery by tandem affinity purification of Arabidopsis protein complexes. Nat. Protoc. **10:** 169–187.

Vermeer, J.E., van Leeuwen, W., Tobeña-Santamaria, R., Laxalt, A.M., Jones, D.R., Divecha, N., Gadella, T.W., Jr., and Munnik, T. (2006). Visualization of PtdIns3P dynamics in living plant cells. Plant J. **47:** 687–700.

Vida, T.A., and Emr, S.D. (1995). A new vital stain for visualizing vacuolar membrane dynamics and endocytosis in yeast. J. Cell Biol. **128:** 779–792.

Vizcaíno, J.A., et al. (2014). ProteomeXchange provides globally coordinated proteomics data submission and dissemination. Nat. Biotechnol. **32:** 223–226.

Walter, M., Chaban, C., Schutze, K., Batistic, O., Weckermann, K., Nake, C., Blazevic, D., Grefen, C., Schumacher, K., Oecking, C., Harter, K., and Kudla, J. (2004). Visualization of protein interactions in living plant cells using bimolecular fluorescence complementation. Plant J. **40:** 428–438.

Wang, P., Xue, L., Batelli, G., Lee, S., Hou, Y.J., Van Oosten, M.J., Zhang, H., Tao, W.A., and Zhu, J.K. (2013). Quantitative phosphoproteomics identifies SnRK2 protein kinase substrates and reveals the effectors of abscisic acid action. Proc. Natl. Acad. Sci. USA **110:** 11205–11210.

Ward, J.J., Sodhi, J.S., McGuffin, L.J., Buxton, B.F., and Jones, D.T. (2004). Prediction and functional analysis of native disorder in proteins from the three kingdoms of life. J. Mol. Biol. **337:** 635–645.

Williams, R.L., and Urbé, S. (2007). The emerging shape of the ESCRT machinery. Nat. Rev. Mol. Cell Biol. **8:** 355–368.

Winter, V., and Hauser, M.T. (2006). Exploring the ESCRTing machinery in eukaryotes. Trends Plant Sci. **11:** 115–123.

Wywial, E., and Singh, S.M. (2010). Identification and structural characterization of FYVE domain-containing proteins of *Arabidopsis thaliana*. BMC Plant Biol. **10:** 157.

Yoshida, T., Mogami, J., and Yamaguchi-Shinozaki, K. (2015). Omics approaches toward defining the comprehensive abscisic acid signaling network in plants. Plant Cell Physiol. **56:** 1043–1052.

Zwiewka, M., Nodzyński, T., Robert, S., Vanneste, S., and Friml, J. (2015). Osmotic stress modulates the balance between exocytosis and clathrin-mediated endocytosis in *Arabidopsis thaliana*. Mol. Plant **8:** 1175–1187.